Tissue-specific roles for Sonic hedgehog signaling in establishing thymus and parathyroid organ fate

Virginia E. Bain[1], Julie Gordon[1], John D. O'Neil[1], Isaias Ramos[1], Ellen R. Richie[2], and Nancy R. Manley[1,3]

[1]Department of Genetics, Paul D. Coverdell Center, 500 DW Brooks Drive, University of Georgia, Athens, GA, 30602

[2]Department of Epigenetics and Molecular Carcinogenesis, University of Texas, M.D. Anderson Cancer Center, Science Park Research Division, Smithville, TX, 78957

[3]Author for correspondence: nmanley@uga.edu, tel. 706-542-5861, fax. 706-583-0691.

Keywords: *Sonic hedgehog*, thymus, parathyroid, endoderm, neural crest, morphogenesis

Abstract

The thymus and parathyroids develop from shared organ primordia derived from third pharyngeal pouch (3rd pp) endoderm. Our previous studies show that *Sonic hedgehog* (*Shh*) null mutants have smaller, aparathyroid primordia in which thymus fate specification extends into the pharynx. SHH signaling is active in both dorsal pouch endoderm and neighboring neural crest mesenchyme, but it is unclear which target tissue of SHH signaling is required for the patterning defects seen in *Shh* mutants. We have taken a genetic approach to this question by ectopically activating or deleting the SHH signal transducer *Smoothened* (*Smo*) in either pharyngeal pouch endoderm or neural crest (NC) mesenchyme. While no individual manipulation recapitulated the *Shh* null mutant phenotype, manipulation of SHH signaling in either the endoderm or NC mesenchyme had direct and indirect effects on both cell types during fate specification and organogenesis. Activation of the SHH pathway throughout the pouch endoderm activated ectopic *Tbx1* expression and partially suppressed the thymus-specific transcription factor *Foxn1*, identifying *Tbx1* as a critical target of SHH signaling in the 3rd pouch. However, ectopic SHH signaling was not sufficient to expand the GCM2 positive parathyroid domain, indicating that multiple inputs, some of which may be independent of SHH signaling, are required for parathyroid fate specification. These data support a model in which SHH signaling plays both positive and negative roles in patterning and organogenesis of the thymus and parathyroids.

Introduction

In mice, thymus and parathyroid organogenesis begins at E9.5 when the third pharyngeal pouch (3rd pp) is formed. The current model for 3rd pp patterning suggests that opposing signaling pathways induce the dorsal parathyroid (Sonic hedgehog, SHH) and ventral thymus (BMP2/4, FGF8/10) domains (Gordon and Manley, 2011). While the parathyroid marker *Gcm2* is expressed at E9.5, the earliest defined thymus specific marker, *Foxn1*, is not detected until E11 (40 somites) in the ventral most regions of the pouch (Gordon et al., 2001). By E11.5 (48 somites) *Foxn1* is strongly expressed throughout the thymus domain of the developing organ primordium (Gordon et al., 2001), and most cells have acquired either a parathyroid or thymus fate.

SHH signaling is active in both the dorsal pouch endoderm and adjacent neural crest (NC) mesenchyme by at least E9.5, during pouch formation (Moore-Scott and Manley, 2005; Grevellec et al., 2011). In the absence of SHH there is no parathyroid domain and *Foxn1* expression expands throughout the pouch and into the pharynx (Moore-Scott and Manley, 2005), although the exact role of SHH signaling in parathyroid fate establishment is not clear (Grevellec et al., 2011). While *Gcm2* is required for survival of the parathyroid domain, it does not appear to be responsible for fate commitment (Liu et al., 2007). In *Gcm2* null mice a *Gcm2* negative domain that expresses *Tbx1* and *CaSR* at E10.5 is present and survives until E12, when it undergoes coordinated apoptosis (Liu et al., 2007). *Tbx1* is a good candidate for mediating the effects of SHH on 3rd pp patterning because it is a known target of SHH signaling in pharyngeal arch mesoderm (Garg et al., 2001; Yamagishi et al., 2003). These data led us to propose that a *Shh-Tbx1-Gcm2* regulatory pathway is responsible for establishing initial parathyroid fate (Liu et al., 2007). Consistent with this model, we showed that TBX1 inhibits *Foxn1* expression when misexpressed in thymic epithelial cells (Reeh et al., 2014).

Both initial patterning and later thymus and parathyroid organogenesis depend on epithelial-mesenchymal interactions between pouch endoderm and NC cells (Gordon and Manley, 2011). *Splotch* mice have a null mutation in *Pax3*, resulting in a loss of NC cells (Conway et al., 2000; Epstein et al., 2000; Pani et al., 2002). E12.5 thymus lobes in S*plotch* embryos are hyperplastic and ectopic (Griffith et al., 2009). Increased thymus size correlates with a decreased parathyroid size, and is due to a shift in the location of the organ domain boundaries in the developing 3rd pp (Griffith et al., 2009). This result showed that signals from NC cells to the developing endodermal primordia determine the location of the border between thymus and parathyroid domains, and thus affect pouch patterning.

In the current study we investigated the respective contributions of SHH signaling within NC mesenchyme and pouch endoderm during 3rd pp patterning and organ development. We used tissue-specific Cre driver strains to selectively delete or ectopically activate SHH signaling in NC mesenchyme or pharyngeal endoderm by expression or activity of the SHH signaling transducer *Smoothened* (*Smo*). Loss of SHH signaling to NC mesenchyme did not shift domain borders (as in *Splotch* mice), but did affect patterning and proliferation of the endodermal primordia. Furthermore, in contrast to *Shh* null embryos, loss of SHH signaling within pouch endoderm did not prevent *Gcm2* expression. These results show that SHH signaling within NC cells or endoderm is sufficient for parathyroid fate specification. We further show that during normal development, establishment of the border between thymus and parathyroid fate involves a transient stage of cell mixing between the two organ fates. The resolution of this cell mixing to non-overlapping organ domains may be mediated by differential cell adhesion, and is dependent on SHH signaling to the NC mesenchyme. This result indicates that epithelial-mesenchymal signals that mediate the establishment of organ borders are SHH dependent. We also show that SHH signaling within the endoderm is sufficient to induce *Tbx1* expression and suppress *Foxn1* expression, but that

this effect is blocked in the most ventral pouch, and is not sufficient to induce *Gcm2*. Our data suggest that high levels of *Bmp4* expression in the most ventral pouch may 'protect' those cells from the effects of ectopic SHH signaling, preventing *Tbx1* expression and thus allowing ventral pouch cells to differentiate as thymus despite enforced *Smoothened* activation.

Materials and Methods

Mice

Smo^{fx}, *Rosa26SmoM2*, *Wnt1Cre*, and *Foxa2Cre^{ERT2}* mice were from The Jackson Laboratory (Bar Harbor, ME), and used to generate *Wnt1Cre;Smo^{fx}* (NCC-specific deletion), *Foxa2Cre^{ERT2};Smo^{fx}* (endoderm-specific deletion), *Wnt1Cre;Rosa26SmoM2* (NCC-specific activation) and *Foxa2Cre^{ERT2};Rosa26SmoM2* (endoderm-specific activation) embryos and littermate controls. Cre-positive and Cre-negative controls were assessed in all experiments; no effects of Cre expression alone were observed. R26Rβgal reporter mice were from The Jackson Laboratory (Bar Harbor, ME). Colonies were maintained on a mixed C57Bl6/J;129Sv genetic background.

The day of the vaginal plug was designated embryonic day 0.5 (E0.5). Embryos were staged by somite number and morphological cues. Genotyping of yolk sac-derived DNA used previously described primers (Danielian et al., 1998; Soriano, 1999; Long et al., 2001; Jeong et al., 2004; Park et al., 2008). Pregnant females from tamoxifen-inducible Cre lines were injected with tamoxifen (Sigma; 3 mg per 40 g body weight) on E5.5. All experiments were approved by the UGA Committee for Animal Use in Research and Education.

Tissue preparation

Embryos for frozen sections were fixed in 4% PFA for 20 minutes (E10.5), or 30 minutes (E11.5-E13.5), washed in PBS, then 20% sucrose, and embedded in OCT. Sections were cut on a cryostat at 8 μm. Embryos collected for paraffin sections were fixed for 1 hour, washed in PBS, dehydrated through an ethanol gradient, permeabilized in xylene, and embedded in paraffin. Embryos collected for *in situ* hybridization (ISH) were kept cold and RNase-free reagents were used. Sections for immunostaining were cut on a Leica RM2155 microtome at 8 μm, and for ISH at 12 μm.

In situ hybridization

Whole mount and paraffin section ISH were performed as described (Manley and Capecchi, 1995; Moore-Scott and Manley, 2005), using mutant embryos and littermate controls. Each probe was analyzed on a minimum of 2-3 embryos per stage. Probes for *Fgf8* (Crossley and Martin, 1995), *Ptch1* (Goodrich et al., 1996), *Tbx1* (Chapman et al., 1996), *Gcm2, Foxn1, Bmp4* (Gordon et al., 2001), and *Fgf10* (Bellusci et al., 1997) were previously described.

Immunostaining

Immunostaining was performed on paraffin embedded or frozen tissue fixed in 4% PFA. Paraffin sections were washed in xylene and rehydrated through an ethanol gradient to dH_2O. For antigen retrieval, tissue was boiled in AR buffer (10 mM sodium citrate pH6, 0.05% Tween20) for 30 minutes and allowed to cool for 20 minutes. Slides were incubated overnight at 4^{o}C in 100 µL 5% donkey serum and 0.05% Triton-X in PBS containing primary antibodies. Slides were washed in PBS and incubated with secondary antibodies in PBS for 1 hour at room temperature in the dark. Slides were washed three times in PBS, with the second wash containing DAPI. Slides were mounted with Fluorogel (EMS). Frozen sections were washed in PBS then incubated with primary and secondary antibodies as above. Primary antibodies were goat anti-Foxn1 (1:200, Santa Cruz sc-23566, G-20), rabbit anti-Gcm2 (1:200, Abcam ab64723), rabbit anti-Tbx1 (1:100, Abcam ab18530), rabbit anti-Cleaved Caspase-3 (1:200, Cell Signaling #9661), rat anti-BrdU (1:10, Serotec OBT0030CX), rat anti-E-cadherin (1:200, Invitrogen 13-1900). Secondary antibodies were DyLight-conjugated (Jackson Immunoresearch).

Cell proliferation

Pregnant female mice were injected intraperitoneally with 5-Bromodeoxyuridine (BrdU, 50 mg/kg body weight) (Sigma) 90 minutes before embryo collection. Embryos were processed for frozen sectioning as above. Sections were fixed in ice-cold acetone for 2 minutes, treated with 2M HCl for 30 minutes, then incubated with rat anti-BrdU antibody (AbD Serotec, 1:10 diluted in PBS+10% donkey serum) overnight at 4°C. Sections were washed 3 times in PBS, and incubated with a DyLight-conjugated donkey anti-rat secondary antibody (Jackson Immunoresearch, 1:1000) for 30 minutes.

In vitro cell aggregation

Thymus-parathyroid primordia were isolated from E12.0 *Gcm2-EGFP* mouse embryos (Condie 2016) then washed in PBS. Tissue was digested to a single cell suspension using 2 mg/ml hyaluronidase, 0.7 mg/ml collagenase and 0.05 mg/ml DNase (Sigma), for 10 minutes at 37°C. Cells were centrifuged, washed in medium (DMEM; 10% FBS; 10% glutamine; 10% pen/strep) then pelleted again. Almost all media was removed and the resulting slurry was pipetted onto a floating filter in a 6-well plate containing culture media. Two days later, the reaggregate was transferred to a v-bottomed 96-well plate containing culture media, incubated for 3 days, harvested, and fixed in 4% PFA for 30 minutes. Tissues were processed through a sucrose gradient and embedded in OCT. Frozen sections (10 μm) were cut and stained with anti-E-cadherin (Invitrogen) and DAPI. To confirm single cell dissociation, reaggregated cells were collected after 24 hours on the floating filter, processed, sectioned, and stained with DAPI.

X-gal staining

Embryos for x-gal staining were processed as described (Gordon et al., 2001). Stained embryos were paraffin embedded and sectioned at 10 μm thickness.

Cell counting

Cell counting was performed manually using images of serial sections taken on a Zeiss Axioplan microscope, using the events feature in AxioVision Rel.4.8 software.

3-D reconstructions

3-D reconstructions were generated from serial sections using SurfDriver WinSurf 4.3 software.

Methodology and Statistics

For phenotypic analysis of mutants we used an initial sample size of 3 embryos (6 primordia; n values refer to primordia number). Additional embryos were analyzed as needed to achieve statistical significance for any observed phenotypes. Significance was determined using an unpaired T test. Controls and mutants were processed in parallel for all experiments; littermate controls were used when possible, otherwise controls and mutants were from the same colony. All results from experiments where one or more embryos or samples had a technical failure (tissue damage, weak or uneven staining) were discarded.

Results

We conditionally deleted *Smo* or induced expression of the constitutively active form *SmoM2* from NC mesenchyme using *Wnt1Cre* (Danielian et al., 1998) or endoderm using *Foxa2*^{CreERT2} (Park et al., 2008). Efficiency of deletion or activation was assessed indirectly

using *Ptch1* expression as an indicator of SHH signaling (Fig.S1). Deletion of *Smo* by *Wnt1Cre* efficiently removed SHH signaling from NC cells surrounding the 3rd pp (Fig.S1D,E), while the tamoxifen-inducible *Foxa2*^{CreERT2} efficiently removed SHH signaling throughout the 3rd pp, but not from the main pharyngeal endoderm (Fig.S1D,F). Similarly, induction of the R26SmoM2 allele using *Wnt1Cre* caused strong upregulation of SHH signaling throughout the pharyngeal arch mesenchyme (Fig.S1G,H), while *Foxa2*^{CreERT2} induced SHH signaling strongly in the pouch endoderm (Fig.S1G,I). While endoderm-specific induction was particularly efficient in the dorsal pouch, we consistently found a few cells in the ventral domain that did not strongly upregulate *Ptch1* (Fig.S1I'). This is consistent with our previously published data showing that in some cases the *Foxa2*^{CreERT2} strain can display low-level inefficient deletion in the 3rd pp (Chojnowski et al., 2014). However, as the number and location of undeleted cells vary between individual pouches, and the phenotypes observed should have cell-autonomous effects, any results that were consistently observed between embryos were unlikely to be significantly affected by the presence of a few cells in which SHH signaling was either not deleted or not upregulated.

SHH signaling to either endoderm or NC is sufficient to specify parathyroid fate

We hypothesized that SHH signaling to NC mesenchyme is responsible for boundary placement between the thymus and parathyroid domains in the 3rd pp, while SHH signaling to 3rd pp endoderm is necessary to establish parathyroid fate. To test this model we deleted *Smo* from either NC mesenchyme (*Wnt1Cre*) (Fig.1B,E) or pharyngeal endoderm (*Foxa2Cre*^{ERT2}) (Fig.1C,F) and examined expression of thymus and parathyroid-specific markers. *Gcm2* expression is absent in *Shh* null embryos (Moore-Scott and Manley, 2005). We were therefore surprised to find that *Gcm2* expression was largely unaffected by tissue-specific loss of SHH signaling. While there were minor differences in overall primordium size, *Gcm2*

was expressed in approximately 25% of the E10.5 3rd pp after deletion of *Smo* from either NC mesenchyme (Fig.1B,E) or endoderm (Fig.1C,F) similar to controls (Fig.1A,D).

We also assessed the expression of *Fgf8* and *Tbx1*, both of which are known targets of SHH signaling (Garg et al., 2001; Yamagishi et al., 2003). Both *Fgf8* and *Tbx1* have restricted expression patterns in the 3rd pp at E10.5, and have been implicated in thymus and/or parathyroid fate specification and organogenesis (Jerome and Papaioannou, 2001; Frank et al., 2002; Manley et al., 2012). No significant differences were seen in the expression of these markers at E10.5 in embryos when *Smo* was deleted from either the endoderm (Fig.S2C,D,K,L) or NC mesenchyme (Fig.S2A,B,I,J). These data indicate that, in contrast to *Shh* null mutants, initial 3rd pp patterning was normal when SHH signaling was selectively deleted in either NC cells or 3rd pp endoderm.

Medial cells within the 3rd pp assort into organ-specific domains

Our previous data showed that in mice, organ fates within the pouch are initiated in the most dorsal (parathyroid) and ventral (thymus) domains, then 'spread' to all cells of the pouch (Gordon et al., 2001; Griffith et al., 2009). To examine this process of 'fate spreading' with greater temporal resolution, we assessed the patterns of FOXN1 and GCM2 expression in wild-type embryos at 1-2 somite intervals from the earliest stage when both FOXN1 and GCM2 are present within the 3rd pp at E11 (40 somites) to E12.5 (60 somites), when the developing thymus and parathyroid organs separate from each other.

At E11 (40 somites; Fig.2A), $GCM2^{+}$ cells are confined to the most dorsal-anterior region and FOXN1 is present in the most ventral-posterior region, with scattered marker-negative cells in both domains. There is also a central region composed of cells that express neither marker (Gordon et al., 2001; Griffith et al., 2009) (Fig.2A, between dotted lines). By 44 somites, the primordium is larger and most epithelial cells have acquired one or the other

organ-specific marker, with FOXN1^{+} or GCM2^{+} cells mixing in the central region (Fig.2B, dotted lines). This mixing is maintained through the 47-somite stage (Fig.2C,D,E), then resolved such that thymus and parathyroid cells assort into distinct domains with a well-defined border. By 56 somites separation of the two organ domains begins (Fig.2F) (Table 1).

These data support a model in which parathyroid and thymus cell fates are initially established at the dorsal and ventral ends of the pouch, respectively. Then, over about one day of embryonic development the marker-negative cells in the central domain undergo a cell fate decision to assume either organ fate, and assort into distinct domains to resolve a clear organ boundary.

Loss of SHH signaling to the NC mesenchyme results in delayed domain resolution

To determine whether SHH signaling to the NC mesenchyme affects organ domain specification, we examined the number and organization of FOXN1^{+} and GCM2^{+} cells in *Wnt1Cre;Smo$^{fx/fx}$* embryos at E11 (40 somites). To quantify patterning phenotypes, we divided the 40-somite stage primordium into five regions from ventral-most to dorsal-most (Fig.3A). In control embryos, all FOXN1^{+} cells were located in the three most ventral regions of the primordium (regions 1-3) (Fig.3B,B'). GCM2^{+} cells were present in the three most dorsal regions of the primordium (regions 3-5). The central region 3 at this stage is the region of 'intermingling' where FOXN1^{+}, GCM2^{+}, and marker-negative cells were all present.

Following deletion of *Smo* from the NC mesenchyme, FOXN1^{+} cells were primarily located in regions 1 and 2 with a few cells in region 3 and none in region 5 (Fig.3C,C',C''), similar to controls (Fig.3B,B',B''). In contrast, GCM2^{+} cells were found within region 2 at a significantly higher frequency than in controls (Fig.3B',C',D). Because of this altered distribution of GCM2^{+} cells, we determined whether the organ boundary resolution at E11.5

was affected (Fig.3E,F). Ectopic GCM2^{+} cells were located within the most ventral domain at E11.5 (Fig.3F'',G); presumably these are related to the cells that were observed in region 2 at 40 somites. The total numbers of FOXN1^{+} and GCM2^{+} cells were similar between *Wnt1Cre;Smo$^{fx/fx}$* embryos and control littermates at E11.5 (48 somites) (Fig. 3H), suggesting that the ectopic GCM2^{+} cells were due to a cell assortment defect rather than mis-specification.

Defects in cell assortment are consistent with changes in E-cadherin expression

The transition from a mixed population of cells to a well-defined border could occur by selective apoptosis, or by cells assorting into uniform populations based on differential cell adhesion. There is little or no apoptosis in the primordia at these stages, making this an unlikely mechanism (Gordon and Manley, 2011). To test whether a defect in differential cell adhesion could underlie this phenotype, we examined E-cadherin expression in the normal primordium and after deletion of *Smo* from the NC mesenchyme. In control embryos E-cadherin was differentially expressed in the thymus and parathyroid domains, with higher levels in FOXN1^{+} cells (Fig.4A,A',A''). In contrast, in the *Wnt1Cre;Smo$^{fx/fx}$* primordia E-cadherin levels did not correspond to the organ domain boundary defined by FOXN1; both high and low levels of E-cadherin were found within FOXN1^{+} cells (Fig.4B,B',B'').

These data are consistent with the idea that cells in the thymus-parathyroid primordium assort into the organ domains according to their cell adhesive properties. The differential cell adhesion model predicts that when different tissues are dissociated, mixed, and reaggregated *in vitro*, they will preferentially assort based on their differential adhesive properties (Steinberg, 1970; Nose et al., 1988; Friedlander et al., 1989). Thymic epithelial cells have previously been shown to use E-cadherin for cell adhesion (Lee et al., 1994; Müller et al., 1997). Since parathyroid cells express a lower level of E-cadherin than cells in

the thymus domain at E11.5 (Fig.4C,C',C''), differential cell adhesion could be the mechanism driving cellular organization during normal development. To test whether the differential expression levels observed were sufficiently different to drive cell assortment based on organ identity, E12.0 primordia from *Gcm2-EGFP* reporter embryos were isolated and dissociated to a single cell suspension, then allowed to reaggregate as a mixed population (Fig.4D). After 4 days in culture, cells were organized into distinct GFP^+ and GFP^- clusters that correlated with low and high E-cadherin levels (Fig.4E,F,G). This result suggests that cells from the thymus-parathyroid primordium can reorganize *in vitro,* consistent with differential cell adhesion.

Taken together, these results suggest that cell assortment in the central domain during normal development may be dependent on differential E-cadherin levels, and that this is influenced by SHH signaling to NC mesenchyme. Differential cell adhesion may mediate both the initial location of parathyroid cell specification and the ability to assort into separate thymus and parathyroid organ domains. It is also possible that inefficient cell segregation is a secondary consequence of the broader domain of cell mixing, resulting in cells being 'trapped' outside their normal organ domain.

Loss of SHH signaling to the endoderm results in an ectopic thymus domain

In contrast to the complete absence of parathyroid domain in the *Shh* null mutants [Moore-Scott, #3646], deletion of *Smo* from the pharyngeal endoderm resulted in comparatively mild effects on 3rd pp patterning and organ development. Only the most dorsal region 5 was abnormal in embryos following loss of SHH signaling to the endoderm, where a small patch of FOXN1 positive cells was present in five out of six primordia examined at 40-41 somites (Fig.5A,C''). These $FOXN1^+$ cells were completely separated from the primary thymus domain in regions 1 and 2 (Fig.5C,C'). By the 48-somite stage, this dorsal $FOXN1^+$

region was continuous with the main FOXN1 domain (Fig.5E), and the total cell number within the primordium was comparable between mutant and control embryos (Fig.5F). Thus, deletion of SHH signaling in pouch endoderm resulted in a mostly normal primordium, except for an abnormal anterior dorsal distribution of FOXN1-expressing cells.

Activation of the SHH pathway in NC mesenchyme delays patterning and suppresses epithelial proliferation

As neither tissue-specific deletion of *Shh* phenocopied either the *Shh* null or *Splotch* mutant LOF phenotypes, we performed gain-of-function (GOF) experiments to test whether ectopic SHH signaling was sufficient to affect the patterning and development of the 3rd pharyngeal pouch. We again looked at pouch patterning and found that early *Tbx1* and *Fgf8* expression was normal at E10.5 when the SHH pathway was activated in the NC mesenchyme (Fig.S2E,F,M,N) and 3rd pp endoderm (Fig.S2G,H,O,P).

Ectopic expression of activated Smoothened (*R26SmoM2*) in NC mesenchyme by *Wnt1Cre* resulted in reduced cell numbers and levels of expression for both FOXN1 and GCM2 at 40 somites. While the anterior-posterior distribution of FOXN1^{+} and GCM2^{+} cells within the five regions was comparable to wild-type (Fig.6A), marker-positive cells were found primarily within the dorsal side of the pouch, with ventral cells largely marker-negative at this stage (Fig.6A,C,C',C''). By the 50-somite stage, all cells within the primordium expressed either FOXN1 or GCM2, indicating delayed marker expression on the ventral side (Fig.6E,E'). The overall primordium size was similar between mutants and controls at 40 somites (Table 2), but by the 50-somite stage was reduced in the mutants (Fig.6F) consistent with reduced proliferation (Fig.S3). Relative parathyroid size was also reduced from 26.7% to 15.7% of the total primordium (Table 3). These results showed that ectopic activation of SHH signaling within NC mesenchyme results in delayed initial cell fate specification and

reduced proliferation within the developing primordium, followed by increased thymus and reduced parathyroid fate specification.

Activation of the SHH pathway in the pouch endoderm results in a reduced FOXN1 domain

We next assessed the effects of ectopic expression of activated Smoothened (*R26SmoM2*) throughout the pharyngeal endoderm using *Foxa2Cre*^{ERT2}. Our initial hypothesis predicted an expanded GCM2 domain within the primordium at the expense of the thymus domain in these mutants. While the FOXN1 domain was restricted to the most ventral region at 40 somites (Fig.7A,C), the number of GCM2 positive cells was similar to controls (Fig.7F). The overall 3rd pp size was normal following activation of the SHH pathway in the pouch endoderm (Table 2). However, the distribution of GCM2^{+} cells was more ventral, extending into region 2 at 40 somites (Fig.7C'). The restriction in FOXN1^{+} cells and normal GCM2^{+} cell numbers resulted in a substantial proportion of the central pouch that expressed neither marker (Fig.7A,C). This delayed patterning was superficially similar to that seen at this stage when the SHH pathway was activated in NC mesenchyme (Fig. 6). However, these phenotypes persisted at 48 somites following SHH pathway activation in the pouch endoderm (Fig. 7E), resulting in a domain of FOXN1 and GCM2 negative cells in the central region (Fig.7E', asterisk).

The number of marker-negative cells plus FOXN1^{+} cells was comparable to the total number of FOXN1^{+} cells in a wild-type pouch at this stage (Fig.7F). This result suggests that this marker-negative region likely represents cells located within the region of the primordium that would normally have been part of the FOXN1^{+} thymus domain, but had failed to turn on *Foxn1*. Thus, ectopic SHH signaling did not lead to an increase in the number of cells expressing *Gcm2* nor did it completely block *Foxn1* expression. Instead,

activation of the pathway prevented *Foxn1* expression from expanding within the central pouch domain.

Ectopic Tbx1 expression corresponds to a suppression of Foxn1

In the *Gcm2* null mutant, a presumptive parathyroid domain that expresses *Tbx1* is present at E11.5 (Liu et al., 2007). Therefore, we tested whether ectopic SHH signaling within the pouch endoderm in *Foxa2Cre^{ERT2};R26SmoM2* embryos induced ectopic *Tbx1* expression. *Tbx1* is normally restricted to the anterior-dorsal domain of the E11.5 pouch (Fig.8B,F,N) (Manley et al., 2004; Liu et al., 2007), co-expressed with *Gcm2* (Fig. 8E,M) and complementary to *Foxn1* (Fig.8A,I,J) In embryos where SHH signaling was activated within the pouch endoderm, *Tbx1* was expressed both in its normal domain with *Gcm2*, and in an ectopic domain in the *Foxn1* and *Gcm2* negative central pouch endoderm at 48 somites, by both RNA expression and protein analysis (Fig.8D,H). In addition, the *Tbx1* expression extended partially into the *Foxn1* domain in the mutants (Fig.8C,D), where *Tbx1* and *Foxn1* levels were inversely correlated (Fig.8L,P). However, *Tbx1* expression did not extend into the most ventral domain (Fig.8D,H). As we previously showed that ectopic expression of *Tbx1* in the thymus domain represses *Foxn1* expression (Reeh et al., 2014), these data suggest that ectopic TBX1 downstream of SHH signaling repressed *Foxn1* in this central domain. Furthermore, cells in the most ventral primordium did not express *Tbx1* and retained *Foxn1* expression, despite ectopic activation of the SHH pathway as shown by *Ptch1* activation (Fig.S1I,I').

Bmp4 and Fgf10 expression are not affected by manipulating SHH signaling

Shh is not expressed in NC mesenchyme adjacent to the 3rd pp. Therefore, in order for SHH signaling in NC mesenchyme to affect the 3rd pp, a second signaling molecule downstream of SHH would need to act directly on the pouch endoderm. Previous studies demonstrated that FGF10 and BMP2/4 act downstream of SHH in palatal mesenchyme (Lan and Jiang, 2009). Both *Fgf10* and *Bmp4* are expressed in the mesenchyme surrounding the pouch, and have been shown to influence parathyroid and thymus organogenesis, although their precise roles are unclear (Gordon and Manley, 2011). Most relevant to this study, *Bmp4* expression is expanded in pouch endoderm of *Shh* null mutants, consistent with the expansion of thymus fate and *Foxn1* expression (Moore-Scott and Manley, 2005).

Fgf10 expression was similar in control and mutant embryos from all four genetic manipulations at E11.5 (Fig.S4), suggesting that FGF10 does not mediate the effects of SHH signaling. Similarly, *Bmp4* expression was not affected by activation of *Smo* in the NC mesenchyme (Fig.9A,B). More significantly, *Bmp4* expression was unaffected by activation of the SHH signaling pathway in the pouch endoderm (Fig.9C,D), even though *Foxn1* expression was restricted to the most ventral primordium. This result is particularly important as BMP4 is implicated in promoting thymus fate. These data suggest that BMP4 expression within and near the central domain could be involved in the failure of *Gcm2* expression to expand after ectopic activation of *Smo* and *Tbx1* in the endoderm.

Pharynx shape is affected by SHH signaling to the neural crest

We noted in the process of analyzing these mutants that it was often difficult to generate comparable planes of section for control and mutant embryos when SHH signaling had been altered in the NC mesenchyme. We have previously shown that the shape of the pharynx is altered in *Shh* null mice (Moore-Scott and Manley, 2005). In wild-type E11.5

embryos, the pharynx has an arch-like shape and the primordium is located adjacent and ventral to the pharynx (Fig.S5A,D,G,J). When SHH signaling was manipulated in 3rd pp endoderm, pharynx shape remained normal (Fig.S5F,L). However, pharynx shape was altered when SHH signaling was manipulated in NC mesenchyme. In the absence of SHH signaling, (*Wnt1Cre;Smo*$^{fx/fx}$), the dorsal-ventral width of the pharynx was increased and the primordium was more dorsally located within the embryo (Fig.S5C). When SHH signaling was activated (*Wnt1Cre;R26SmoM2*), the pharynx was flattened, placing the primordium more laterally (Fig.S5I). These data indicate that SHH signaling to NC mesenchyme helps to shape the pharynx. These shape changes could place the different regions of the pouch into new signaling environments, indirectly influencing 3rd pp patterning.

Discussion

The mechanisms by which the 3rd pp is patterned into thymus and parathyroid fates remain poorly understood. We previously showed that SHH is required to specify the parathyroid domain in the 3rd pp, and that while *Shh* itself is not expressed in the pouch, cells in the dorsal pouch endoderm and the neighboring NC mesenchyme undergo SHH signaling (Moore-Scott and Manley, 2005; Gordon and Manley, 2011). Furthermore, inhibition of SHH signaling in the chick resulted in a failure to initiate *Gcm2* expression and enhanced *Bmp4* expression (Grevellec et al, 2011), consistent with the *Shh* null mouse phenotype (Moore-Scott and Manley, 2005). In the current study we used tissue-specific GOF and LOF mouse mutants to dissect the tissue-specific roles of SHH signaling during 3rd pp patterning. Interestingly, neither NC- nor endoderm-specific deletion of SHH signaling recapitulated the *Shh* null phenotype, suggesting that SHH signaling within either of these cell types is sufficient for parathyroid fate specification. We also showed that ectopic SHH signaling in pouch endoderm induced *Tbx1* and suppressed *Foxn1* expression in the medial pouch, but

was not sufficient to induce *Gcm2* expression in those cells. Finally, the most ventral pouch cells specified thymus fate and turned on *Foxn1* despite enforced SHH signaling. Taken together, these results indicate that cells in the dorsal and ventral 3rd pp are differentially sensitive to levels of SHH signaling, and that this is part of a complex and robust signaling network that controls cell fate establishment during thymus and parathyroid development.

SHH signaling in both the pouch endoderm and neural crest-derived mesenchyme contribute to parathyroid fate

We propose a model (Fig. 10) in which SHH is necessary but not sufficient for parathyroid fate. In the absence of SHH, *Gcm2* is not expressed and parathyroids are absent (Moore-Scott and Manley, 2005; Grevellec et al, 2011). Interestingly, SHH signaling in either the endoderm or NC mesenchyme alone was sufficient but not necessary for *Gcm2* expression and parathyroid fate establishment. It is unlikely that these phenotypes are caused by SHH signaling occurring prior to Cre-mediated deletion because *Foxa2Cre^{ERT2}* was activated at E5.5 prior to 3rd pouch formation, and *Wnt1Cre* acts prior to NC cell migration. It is formally possible, but unlikely, that *Gcm2* expression is dependent on a Smo-independent role for SHH, in which case deleting *Smo* would not recapitulate the *Shh* null phenotype (Jenkins, 2009). It is also possible that another cell type is involved, although it is unclear at this point what cell type that would be. We believe that the most plausible explanation is that SHH signaling to either the endoderm or mesenchyme alone is sufficient to promote *Gcm2* expression in the anterio-dorsal 3rd pp. In the endoderm this could be by direct signaling, but in the mesenchyme there would have to be a second, as yet unidentified, signal acting downstream of *Shh*. Taken together, these data demonstrate that both parathyroid fate and *Gcm2* expression are controlled by multiple factors acting directly within the endoderm

downstream of SHH signaling as well as indirectly from the adjacent NC-derived mesenchyme.

SHH signaling to the NC mesenchyme regulates E-cadherin expression, affecting organization

When SHH signaling was deleted in the neural crest mesenchyme, we observed a phenotype wherein a subset of $Gcm2^{+}$ cells were mixed with $Foxn1^{+}$ cells in a more ventral location. This phenotype is reminiscent of an intermingling phenotype seen in the spinal cord of mutants for Gli3, a negative regulator of SHH signaling. In Gli3 mutants, V2 neurons intermingle with $En1^{+}$ V1 neurons (Persson et al., 2002). However, while these two phenotypes appear similar, they likely arise via different mechanisms. The intermingling in the Gli3 mutant spinal cord is likely due to mis-specification, while that seen in the *Wnt1Cre;Smo*$^{fx/fx}$ mutants is likely a cell assortment defect, due to mis-regulation of E-cadherin. During normal development, we showed that E-cadherin levels are different between the thymus and parathyroid domains and that these cells are capable of reorganizing by homotypic adhesion. In the *Wnt1Cre;Smo*$^{fx/fx}$ mutants, loss of SHH signaling to the neural crest led to misregulation of E-cadherin levels in the primordium, resulting in cells that were unable to sort correctly. The fact that cell numbers were unchanged in these mutant primordia also supports a cell sorting defect, rather than a cell fate switch.

Ectopic SHH signaling and Tbx1 expression are not sufficient to induce Gcm2

Ectopic activation of the SHH pathway in the thymus domain caused a ventral expansion of *Tbx1* expression and suppression of *Foxn1* expression within the central pouch. This result is consistent with our previous study showing that ectopic activation of *Tbx1* in the ventral thymus domain inhibited *Foxn1* expression, but failed to induce *Gcm2* (Reeh, et

al., 2014). There are two possible reasons why *Gcm2* expression did not expand. First, it is possible that a SHH-independent signal acts together with the SHH signaling pathway. One candidate for this pro-parathyroid signal is FGF10, which is expressed in the proximal NC mesenchyme adjacent to the parathyroid domain in the 3rd pouch (Gardiner et al., 2012), and is unaffected in all of the SHH pathway mutants examined in the current study. Also, *Fgf10* null mutants have reduced parathyroid size (JG and NM, unpublished data), further supporting a role for FGF10 in parathyroid development. Second, it is possible that an inhibitory signal in the medial endoderm or surrounding mesenchyme, such as BMP4, dominates over SHH signaling in that middle region of the 3rd pp. SHH and BMP4 work in opposition in many developmental contexts to pattern tissues and organs, and there is evidence to support a similar role in patterning thymus and parathyroid fate within the 3rd pouch (Moore-Scott and Manley, 2005; Gordon and Manley, 2011). We found that forced activation of the SHH signaling pathway in either NC mesenchyme or pouch endoderm did not inhibit *Bmp4* expression within the pouch or in the surrounding mesenchyme. Therefore, BMP4 signaling could act to prevent ectopic parathyroid fate specification and *Gcm2* expression in the central and ventral pouch. BMP4 dominance over SHH signaling within the pouch is also consistent with the establishment of both thymus fate and *Foxn1* expression in the most ventral pouch, even in the presence of enforced expression of constitutively activated *Smoothened*. Clearly it is only the ventral-most cells in the prospective thymus domain that are resistant to SHH-mediated activation of *Tbx1* expression, which allows/enables these cells to maintain *Foxn1* expression, even in the presence of SHH signaling. Whether BMP4 or another unknown dominant signal from the ventral 3rd pp and/or NC mesenchyme antagonizes SHH signaling remains to be determined.

In conclusion, our data show that cells in the 3rd pp endoderm are sensitive to both direct SHH signaling within the pouch and indirect SHH signaling from the NC mesenchyme. The most striking phenotype was obtained when SHH signaling was ectopically induced in the ventral 3rd pp endoderm. Despite the concomitant ventral expansion of *Tbx1* and suppression of *Foxn1* expression, *Gcm2* was not turned on; furthermore, the most ventral cells were completely insensitive to ectopic SHH signaling. These data show that even high levels of ectopic SHH signaling cannot completely change the organ-specific fates of cells within the 3rd pouch. Therefore, a robust network of signaling and transcriptional mechanisms exists, likely including SHH, BMP, FGF and TBX1, which collaborate to establish organ-specific fates within the developing 3rd pharyngeal pouch.

Acknowledgements

We thank Brian Condie for helpful discussion and suggestions; Michelle Dookwah for assisting with the work on 3rd pouch separation.

Funding

This work was supported by National Institutes of Health grants R01HD056315 and R01AI107096 to E.R. and N.M.

Competing interests statement

The authors declare no competing financial interests.

Author contribution

V.B. designed the experiments and performed the analysis under the supervision of N.M; J.O. confirmed results and contributed images to Figs. 2, 8, and 9; J.G. contributed images to Fig. 3; J.G. and I.R. contributed Fig. S3; E.R. and N.M. conceived the project; V.B. J.G. E.R. and N.M. wrote and edited the manuscript.

References

Bellusci, S., Grindley, J., Emoto, H., Itoh, N. and Hogan, B. L. (1997) 'Fibroblast growth factor 10 (FGF10) and branching morphogenesis in the embryonic mouse lung', *Development* 124(23): 4867-78.

Chapman, D. L., Garvey, N., Hancock, S., Alexiou, M., Agulnik, S. I., Gibson-Brown, J. J., Cebra-Thomas, J., Bollag, R. J., Silver, L. M. and Papaioannou, V. E. (1996) 'Expression of the T-box family genes, Tbx1-Tbx5, during early mouse development', *Dev Dyn* 206(4): 379-90.

Chojnowski, J. L., Masuka, K., Trau, H. A., Thomas, K., Capecchi, M. and Manley, N. R. (2014) 'Multiple roles for HOXA3 in regulating thymus and parathyroid differentiation and morphogenesis in mouse', *Development* 141(19):3697-708.

Condie, B. (2016) 'The untapped potential of the GENSAT mice-A valuable resource for developmental biology', *Genesis* 54(5): 245-56.

Conway, S. J., Bundy, J., Chen, J., Dickman, E., Rogers, R. and Will, B. M. (2000) 'Decreased neural crest stem cell expansion is responsible for the conotruncal heart defects within the splotch (Sp(2H))/Pax3 mouse mutant', *Cardiovasc Res* 47(2): 314-28.

Conway, S. J., Henderson, D. J., Kirby, M. L., Anderson, R. H. and Copp, A. J. (1997) 'Development of a lethal congenital heart defect in the splotch (Pax3) mutant mouse', *Cardiovasc Res* 36(2): 163-73.

Crossley, P. H. and Martin, G. R. (1995) 'The mouse Fgf8 gene encodes a family of polypeptides and is expressed in regions that direct outgrowth and patterning in the developing embryo', *Development* 121(2): 439-451.

Danielian, P. S., Muccino, D., Rowitch, D. H., Michael, S. K. and McMahon, A. P. (1998) 'Modification of gene activity in mouse embryos in utero by a tamoxifen-inducible form of Cre recombinase', *Curr Biol* 8(24): 1323-6.

Epstein, J. A., Li, J., Lang, D., Chen, F., Brown, C. B., Jin, F., Lu, M. M., Thomas, M., Liu, E., Wessels, A. et al. (2000) 'Migration of cardiac neural crest cells in Splotch embryos', *Development* 127(9): 1869-78.

Frank, D. U., Fotheringham, L. K., Brewer, J. A., Muglia, L. J., Tristani-Firouzi, M., Capecchi, M. R. and Moon, A. M. (2002) 'An Fgf8 mouse mutant phenocopies human 22q11 deletion syndrome', *Development* 129(19): 4591-603.

Franz, T. (1989) 'Persistent truncus arteriosus in the Splotch mutant mouse', *Anat Embryol (Berl)* 180(5): 457-64.

Friedlander, D. R., Mege, R.M., Cunningham, B. A. and Edelman, G. M. (1989) 'Cell sorting-out is modulated by both the specificity and amount of different cell adhesion molecules (CAMs) expressed on cell surfaces' *Proc. Natl. Acad. Sci.* 86: 7043-7047.

Gardiner, J. R., Jackson, A. L., Gordon, J., Lickert, H., Manley, N. R. and Basson, M. A. (2012) 'Localised inhibition of FGF signalling in the third pharyngeal pouch is required for normal thymus and parathyroid organogenesis', *Development* 139(18): 3456-66.

Garg, V., Yamagishi, C., Hu, T., Kathiriya, I. S., Yamagishi, H. and Srivastava, D. (2001) 'Tbx1, a DiGeorge syndrome candidate gene, is regulated by sonic hedgehog during pharyngeal arch development', *Dev Biol* 235(1): 62-73.

Goodrich, L. V., Johnson, R. L., Milenkovic, L., McMahon, J. A. and Scott, M. P. (1996) 'Conservation of the hedgehog/patched signaling pathway from flies to mice: induction of a mouse patched gene by Hedgehog', *Genes Dev* 10(3): 301-12.

Gordon, J., Bennett, A. R., Blackburn, C. C. and Manley, N. R. (2001) 'Gcm2 and Foxn1 mark early parathyroid- and thymus-specific domains in the developing third pharyngeal pouch', *Mech Dev* 103(1-2): 141-3.

Gordon, J. and Manley, N. R. (2011) 'Mechanisms of thymus organogenesis and morphogenesis', *Development* 138(18): 3865-78.

Gordon, J., Patel, S. R., Mishina, Y. and Manley, N. R. (2010) 'Evidence for an early role for BMP4 signaling in thymus and parathyroid morphogenesis', *Dev Biol* 339(1): 141-54.

Grevellec, A., Graham, A. and Tucker, A. S. (2011) 'Shh signalling restricts the expression of Gcm2 and controls the position of the developing parathyroids', *Dev Biol* 353(2): 194-205.

Griffith, A. V., Cardenas, K., Carter, C., Gordon, J., Iberg, A., Engleka, K., Epstein, J. A., Manley, N. R. and Richie, E. R. (2009) 'Increased thymus- and decreased parathyroid-fated organ domains in Splotch mutant embryos', *Dev Biol* 327(1): 216-27.

Jeong, J., Mao, J., Tenzen, T., Kottmann, A. H. and McMahon, A. P. (2004) 'Hedgehog signaling in the neural crest cells regulates the patterning and growth of facial primordia', *Genes Dev* 18(8): 937-51.

Jenkins D. (2009) 'Hedgehog signalling: emerging evidence for non-canonical pathways', *Cell Signal.* 21:1023–34.

Jerome, L. A. and Papaioannou, V. E. (2001) 'DiGeorge syndrome phenotype in mice mutant for the T-box gene, Tbx1', *Nat Genet* 27(3): 286-91.

Jiang, X., Rowitch, D. H., Soriano, P., McMahon, A. P. and Sucov, H. M. (2000) 'Fate of the mammalian cardiac neural crest', *Development* 127(8): 1607-16.

Lan, Y. and Jiang, R. (2009) 'Sonic hedgehog signaling regulates reciprocal epithelial-mesenchymal interactions controlling palatal outgrowth', *Development* 136(8): 1387-96.

Lee MG, Sharrow SO, Farr AG, Singer A, Udey MC. (1994) 'Expression of the homotypic adhesion molecule E-cadherin by immature murine thymocytes and thymic epithelial cells.', *J Immunol.* 152(12):5653-9.

Liu, Z., Yu, S. and Manley, N. R. (2007) 'Gcm2 is required for the differentiation and survival of parathyroid precursor cells in the parathyroid/thymus primordia', *Dev Biol* 305(1): 333-46.

Long, F., Zhang, X. M., Karp, S., Yang, Y. and McMahon, A. P. (2001) 'Genetic manipulation of hedgehog signaling in the endochondral skeleton reveals a direct role in the regulation of chondrocyte proliferation', *Development* 128(24): 5099-108.

Machado, A. F., Martin, L. J. and Collins, M. D. (2001) 'Pax3 and the splotch mutations: structure, function, and relationship to teratogenesis, including gene-chemical interactions', *Curr Pharm Des* 7(9): 751-85.

Manley, N. R. and Capecchi, M. R. (1995) 'The role of Hoxa-3 in mouse thymus and thyroid development', *Development* 121(7): 1989-2003.

Manley, N. R., Selleri, L., Brendolan, A., Gordon, J., and Cleary, M. L. (2004) 'Abnormalities of caudal pharyngeal pouch development in Pbx1 knockout mice mimic loss of Hox3 paralogs', *Dev. Biol.* 276, 301-312.

Manley, N. R., Richie, E. R., Blackburn, C. C., Condie, B. G. and Sage, J. (2012) 'Structure and function of the thymic microenvironment', *Front Biosci* 17: 2461-77.

Moore-Scott, B. A. and Manley, N. R. (2005) 'Differential expression of Sonic hedgehog along the anterior-posterior axis regulates patterning of pharyngeal pouch endoderm and pharyngeal endoderm-derived organs', *Dev Biol* 278(2): 323-35.

Müller KM, Luedecker CJ, Udey MC, Farr AG. (1997) ' Involvement of E-cadherin in thymus organogenesis and thymocyte maturation', *Immunity* 3:257-64.

Nose, A., Nagafuchi, A. and Takeichi, M. (1988) 'Expressed recombinant cadherins mediate cell sorting in model systems' *Cell* 54: 993-1001.

Pani, L., Horal, M. and Loeken, M. R. (2002) 'Rescue of neural tube defects in Pax-3-deficient embryos by p53 loss of function: implications for Pax-3- dependent development and tumorigenesis', *Genes Dev* 16(6): 676-80.

Park, E. J., Sun, X., Nichol, P., Saijoh, Y., Martin, J. F. and Moon, A. M. (2008) 'System for tamoxifen-inducible expression of cre-recombinase from the Foxa2 locus in mice', *Dev Dyn* 237(2): 447-53.

Persson, M.,Stamataki, D.,te Welscher, P.,Andersson, E.,Böse, J.,Rüther, U.,Ericson, J. and Briscoe, J. (2002) 'Dorsal-ventral patterning of the spinal cord requires Gli3 transcriptional repressor activity', *Genes Dev* 16, 2865-2878.

Patel, S. R., Gordon, J., Mahbub, F., Blackburn, C. C. and Manley, N. R. (2006) 'Bmp4 and Noggin expression during early thymus and parathyroid organogenesis', *Gene Expr Patterns* 6(8): 794-9.

Reeh, K.A., Cardenas, K.T., Bain, V.E., Liu, Z., Laurent, M., Manley, N.R., and Richie, E.R. (2014) 'Ectopic TBX1 supresses thymic epithelial cell differentiation and proliferation during thymus organogenesis', *Development* (141): 2950-2958.

Soriano, P. (1999) 'Generalized lacZ expression with the ROSA26 Cre reporter strain', *Nat Genet* 21(1):70-1.

Steinberg, M.S. (1970) 'Does differential adhesion govern self-assembly processes in histogenesis? Equilibrium configurations and the emergence of a hierarchy among populations of embryonic cells' *J. Exp. Zool.* 173: 395-434.

Yamagishi, H., Maeda, J., Hu, T., McAnally, J., Conway, S. J., Kume, T., Meyers, E. N., Yamagishi, C. and Srivastava, D. (2003) 'Tbx1 is regulated by tissue-specific forkhead proteins through a common Sonic hedgehog-responsive enhancer', *Genes Dev* 17(2): 269-81.

Tables

Table 1. Intermingling between FOXN1- and GCM2-positive cells in the wild-type primordium decreases after 48 somites

Somite number	$FOXN1^+$ cells in the dorsal domain	$GCM2^+$ cells in the ventral domain
39	0	0
40	1.75 +/- 0.9	3.25 +/- 1
41	0.17 +/- 0.2	1.17 +/- 1
42	10.75 +/- 1.5	6.75 +/- 1.3
45	15 +/- 4.0	9 +/- 4.2
46	12.5 +/- 1.5	5
47	18 +/- 2	8.33 +/- 1.2
48	19.29 +/- 2.7	6.86 +/- 0.8
49	8 +/- 1.6	3.75 +/- 0.5
50	7 +/- 1	4
56	0	0
60	0	0

Table 2. Manipulating SHH signaling does not alter primordium size at 40 somites

	Effect of genetic manipulation	Primordium size at 40 somites ($\mu m^{3)}$
Control	-	1.341+/- 6.21E-05
Wnt1Cre;Smo^{fx}	Loss of SHH signaling to NC mesenchyme	1.465+/- 4.26E-05
Foxa2Cre^{ERT2};Smo^{fx}	Loss of SHH signaling to endoderm	1.267+/- 4.36E-05
Wnt1Cre;R26SmoM2	Ectopic SHH signaling within NC mesenchyme	1.715+/- 3.50E-04
Foxa2Cre^{ERT2};R26SmoM2	Ectopic SHH signaling within endoderm	1.407+/- 7.93E-05

Table 3. Percentage of the pouch comprised of FOXN1 and GCM2 domains in SHH signaling mutants compared to the *Splotch* mouse at E11.5

	Controls[1]		Mutants	
	Foxn1 domain	Gcm2 domain	Foxn1 domain	Gcm2 domain
Wnt1Cre;Smo^{fx}	73.4^{+}/-3.8%	26.6^{+}/-1.6%	72.8^{+}/-2.2%	27.2^{+}/-1.1%
Foxa2Cre^{ERT2};Smo^{fx}	70.0^{+}/-8.0%	30.0^{+}/-2.4%	72.3^{+}/-3.8%	27.7^{+}/-3.4%
Wnt1Cre;R26SmoM2	73.3^{+}/-4.6%	26.7^{+}/-3.4%	84.0^{+}/-5.1%	16.0^{+}/-2.2%
Foxa2Cre^{ERT2};R26SmoM2	71.7^{+}/-3.8%	28.3^{+}/-1.4%	41.9^{+}/-3.6%	26.0^{+}/-3.1%
Splotch[2]	71%	29%	78%	22%

[1]Controls in all cases are littermates, independently staged to within 2 somites.
[2]Data from (Griffith et al., 2009).

Figures

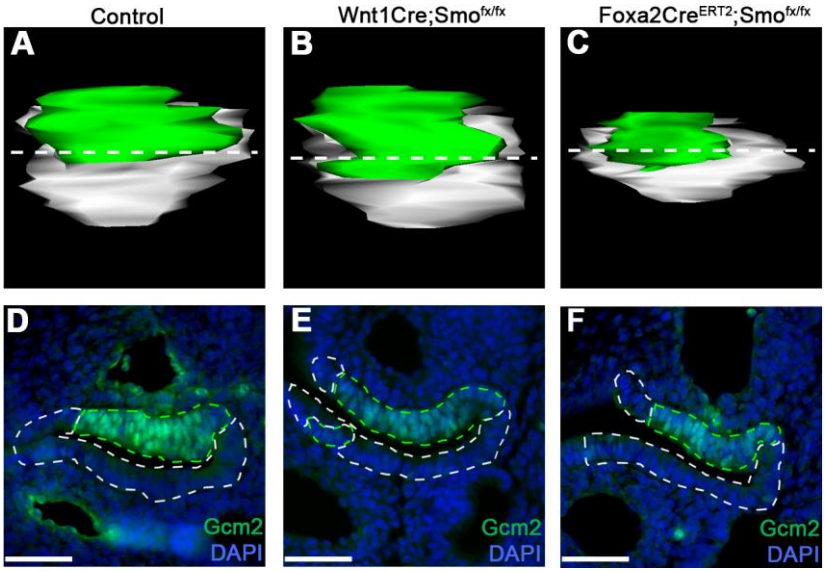

Figure 1. GCM2 expression in E10.5 *Smoothened* loss-of-function mutants. **A-C:** 3-D reconstructions of serial coronal sections from E10.5 embryos stained with anti-GCM2. Genotypes indicated above each column (n=3/genotype). Up is dorsal; anterior surface is shown. Dashed lines in **A-C** indicate position of sections in **D-F** showing representative sections from each reconstruction. $GCM2^{+}$ regions are outlined in green; unstained pouch endoderm is outlined in white. Scale bar: 50 μm.

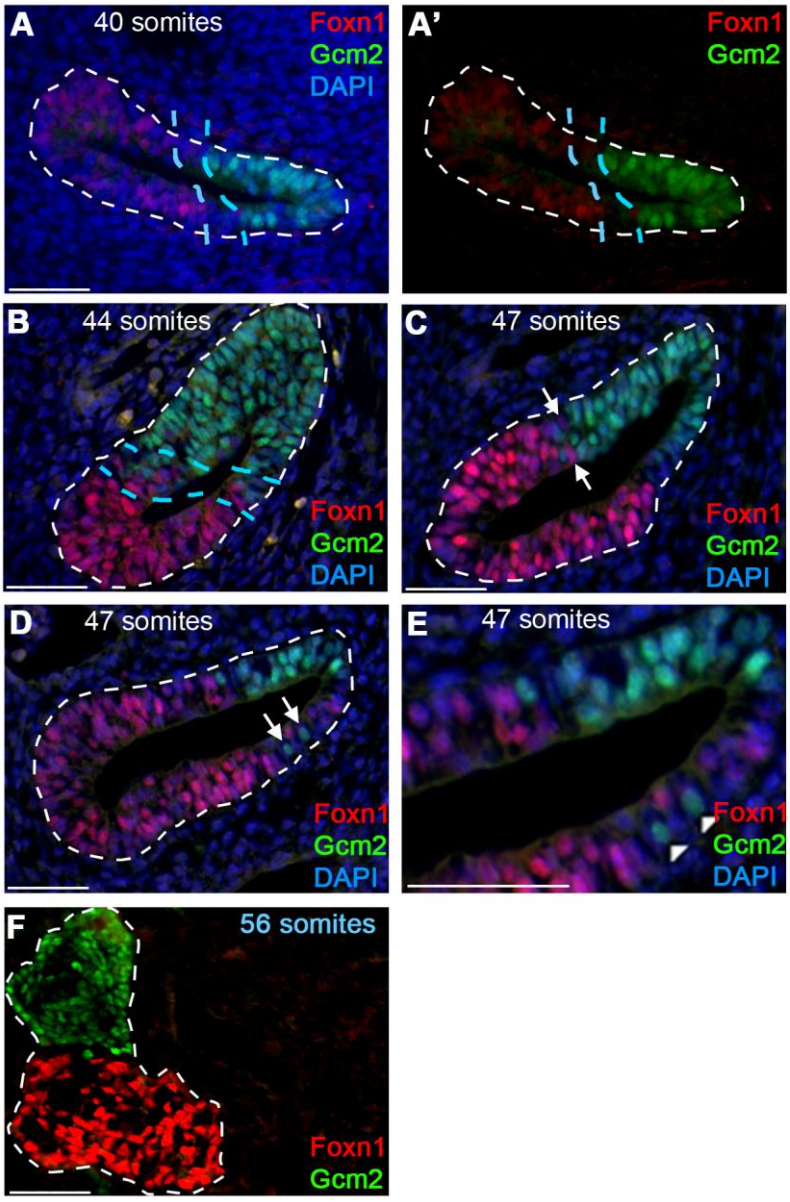

Figure 2. Pouch patterning between E11 and E12. **A-E:** Sagittal sections stained with anti-GCM2 (green), anti-FOXN1 (red), and DAPI (blue). Somite stages are indicated. **A:** Dashed line highlights central region of marker-negative cells. **A'**: Image from A without DAPI. **B-E:** Arrows indicate regions of cell mixing. **E:** Higher magnification of **D**. **F:** Transverse section through primordium from a 56-somite stage embryo. (n=2/stage). Scale bars: 50 μm.

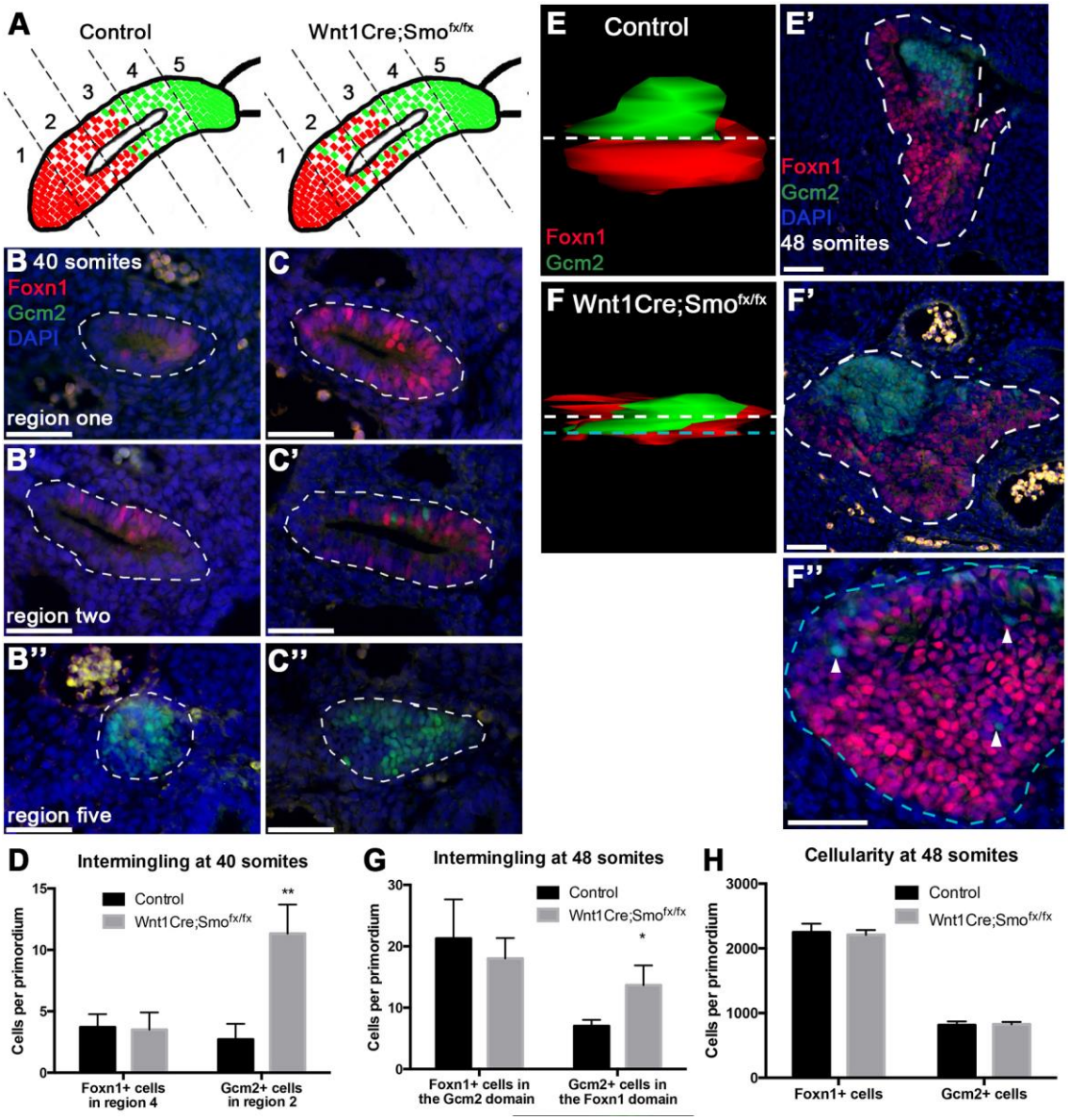

Figure 3. Deletion of *Smoothened* from NC mesenchyme. **A:** Cartoons illustrating distribution of GCM2$^+$ (green) and FOXN1$^+$ (red) cells within the primordium for each genotype from a sagittal view. Primordia were divided into five regions from ventral to dorsal. White indicates cells that express neither marker. **B-C'':** Coronal sections and through 40-somite stage embryos stained with anti-GCM2 and anti-FOXN1. Representative sections from region 1 (**B,C**), 2 (**B',C'**), and 5 (**B'',C''**) are shown for each genotype. Primordia are outlined. Yellow cells outside of the primordia are autofluorescent red blood cells. Scale bar: 50 μm. **D:** Number of ectopic cells within regions 2 and 4 for control (n=10) and

Wnt1Cre;Smo$^{fx/fx}$ (n=6) embryos. mean+s.e.m. t-test **P < 0.01. **E-F:** 3-D reconstructions of transverse sections (**E'-F"**). Primordia are outlined. Dashed white line indicates position of section shown in adjacent panel (**E',F'**). **F'':** Posterior transverse section through primordium from a *Wnt1Cre;Smo*$^{fx/fx}$ embryo, showing GCM2^{+} cells in the FOXN1^{+} domain (arrowheads). Turquoise line in **F** indicates position of **F"** section. Anterior is up; dorsal surface is facing. Scale bar: 50 μm. **G:** FOXN1^{+} or GCM2^{+} cells separated from their respective domains by at least 16 μm in 48-somite stage control and *Wnt1Cre;Smo*$^{fx/fx}$ mutant embryos. mean+s.e.m. t-test *P < 0.05. **H:** Total number of cells in each primordium in somite-matched mutants (n=6) and littermate controls (n=4). mean+s.e.m. t-test. Scale bars: 50 μm

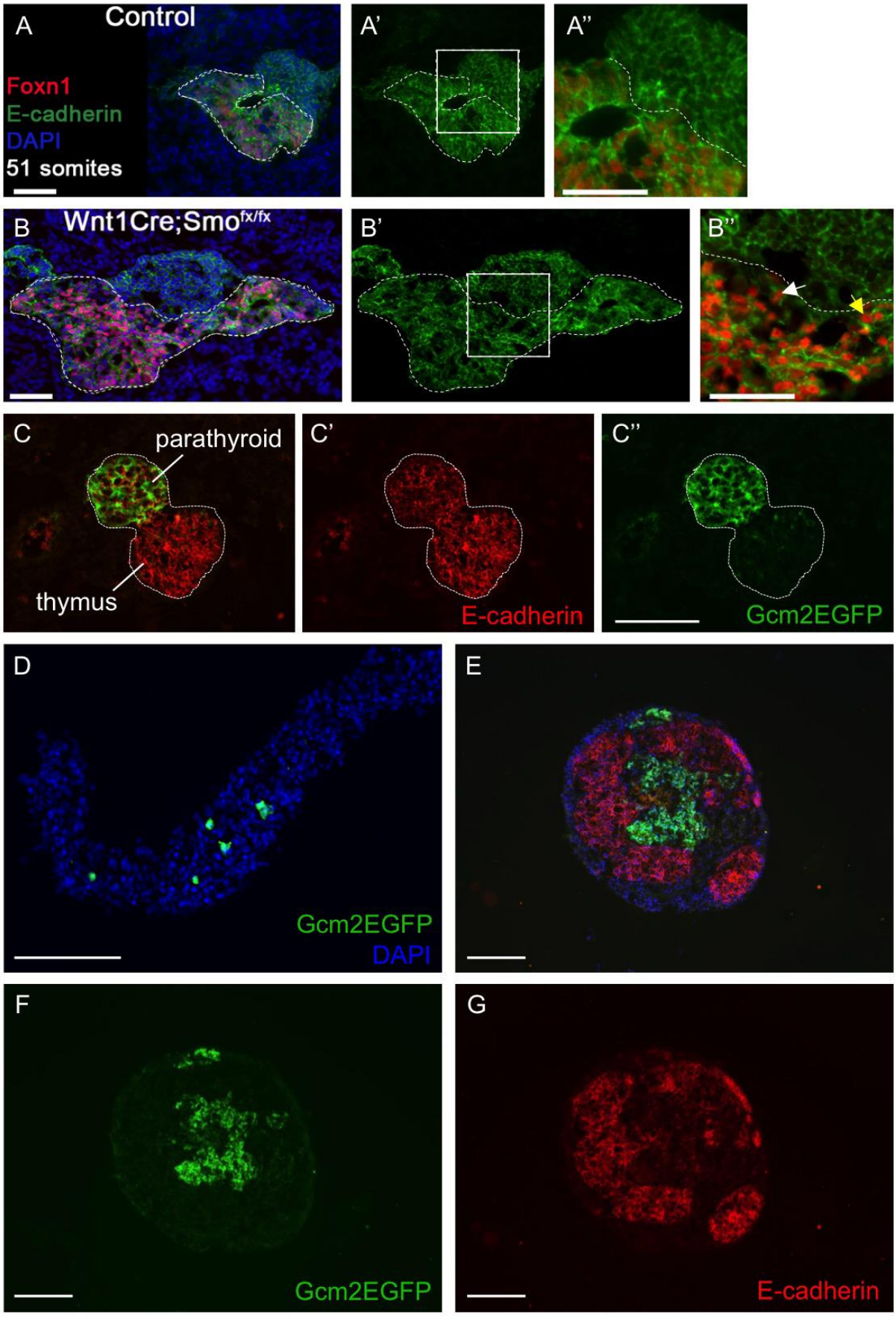

Figure 4. Differential E-cadherin levels are associated with organ-specific cell sorting. **A-B:** Transverse sections through primordia from control (**A**) and *Wnt1Cre;Smo*$^{fx/fx}$ mutant (**B**) embryos at 51 somites stained with anti-E-cadherin (green), anti-FOXN1 (red) and DAPI (blue). FOXN1^{+} domain of each primordium is outlined. **A'** and **B'** are E-cadherin-only images of **A** and **B**, respectively. White boxes in **A'** and **B'** indicate location of images in **A"** and **B"**, respectively. Dotted lines in **A"** and **B"** delineate the border between FOXN1^{+} and FOXN1^{-} domains. White arrow in **B"** indicates a FOXN1^{+};E-cadherin^{lo} cell. Yellow arrow in **B"** indicates a FOXN1^{+};E-cadherin^{hi} cell. **C:** Transverse section through E12.0 *Gcm2-EGFP* primordium (outlined) showing differential E-cadherin levels between the thymus and parathyroid domains. **D:** Dissociated and reaggregated cells from E12.0 thymus-parathyroid primordia after 24-hour culture, showing dispersed GFP^{+} cells. **E-G:** Section through a reaggregate culture after 5 days in culture, showing GFP^{+} cells in clusters (**F**), correlates with E-cadherin levels (**G**). (n=3). Scale bars: 50 μm.

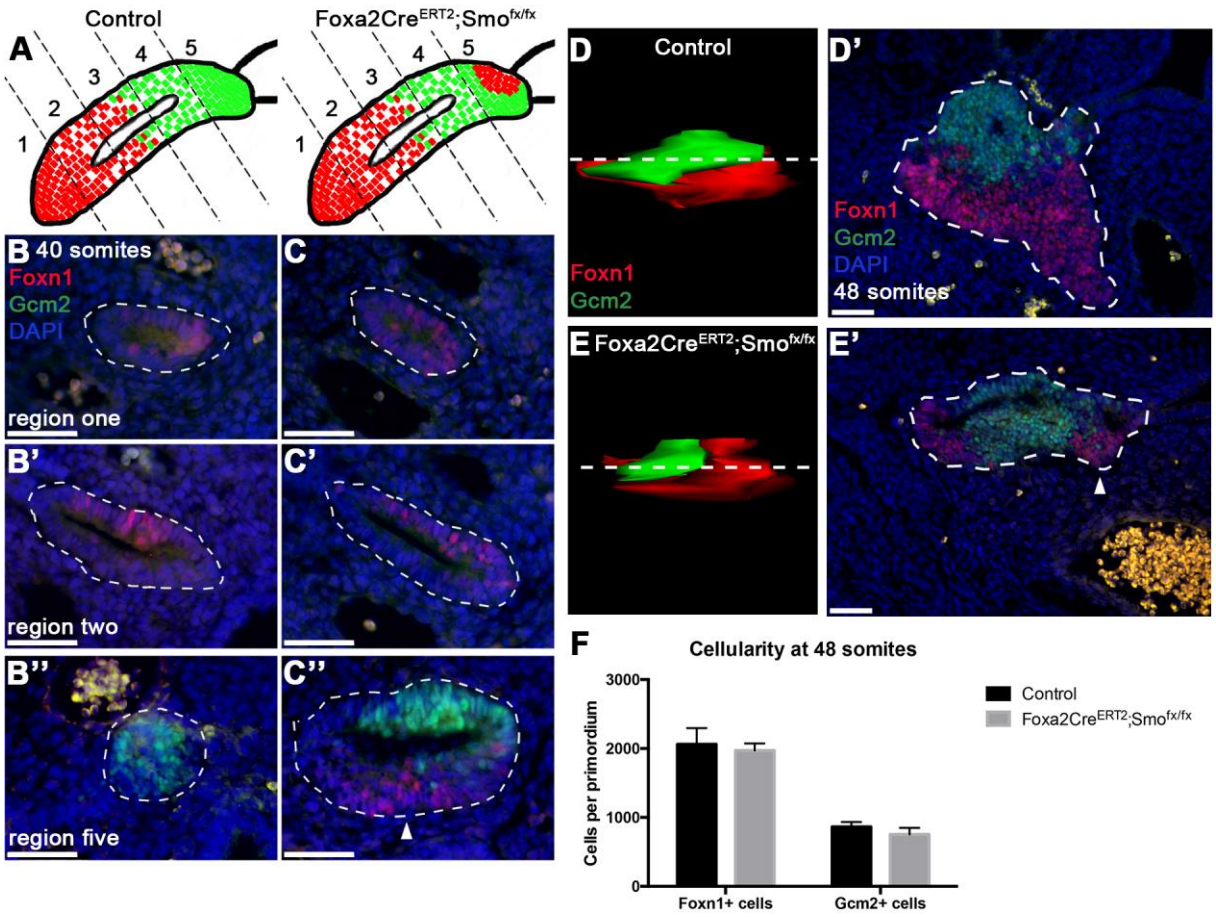

Figure 5. Deletion of *Smoothened* from pouch endoderm. All sections were stained with antibodies against GCM2 (green) and FOXN1 (red); primordia are outlined. **A:** Cartoons illustrating distribution of $GCM2^{+}$ and $FOXN1^{+}$ cells within the primordium for each genotype, sagittal view. Primordia were divided into five equal regions from ventral to dorsal. White indicates cells that express neither marker. **B-C'':** Coronal sections through 40-somite stage embryos. Representative sections from regions 1 (**B,C**), 2 (**B',C'**), and 5 (**B'',C''**) are shown for each genotype. Primordia are outlined. Scale bar: 50 μm. **D-E:** Transverse sections. Primordia are outlined. 3-D reconstructions of each primordium (**D,E**). Dashed line indicates position of section in adjacent panel (**D',E'**). Anterior is up; dorsal surface is facing. Scale bar: 50 μm. F: Total number of cells in each primordium in somite-matched mutants (n=6) and littermate controls (n=4). mean+s.e.m t-test.

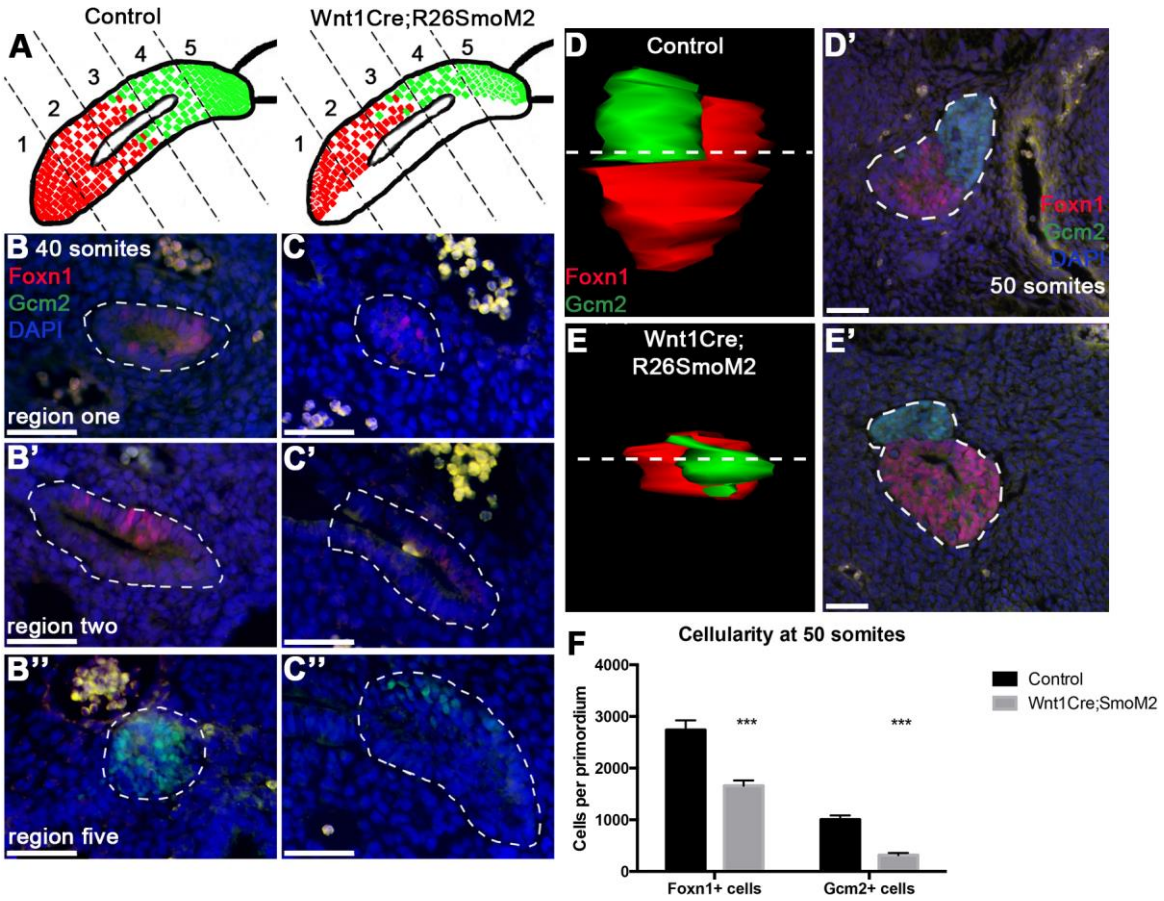

Figure 6. Ectopic activation of SHH signaling in NC mesenchyme. All sections were stained with antibodies against GCM2 (green) and FOXN1 (red); primordia are outlined. **A:** Cartoons illustrating distribution of $GCM2^{+}$ and $FOXN1^{+}$ (red) cells for each genotype from a sagittal view. Primordia were divided into five equal regions from ventral to dorsal. White indicates cells that express neither marker. **B-C'':** Coronal sections through 40-somite stage embryos. Representative sections from regions 1 (**B,C**), 2 (**B',C'**), and 5 (**B'',C''**) are shown for each genotype. Scale bar: 50 μm. **D-E':** 3-D reconstructions (**D,E**) and representative transverse sections of 48 somite primordia (**D',E'**). Dashed line indicates position of section shown in adjacent panel (**D',E'**). Anterior is up; dorsal surface is facing. Scale bar: 50 μm. **F:** Total number of cells in each primordium in somite-matched mutants (n=6) and littermate controls (n=4). mean+s.e.m. t-test ***P < 0.001.

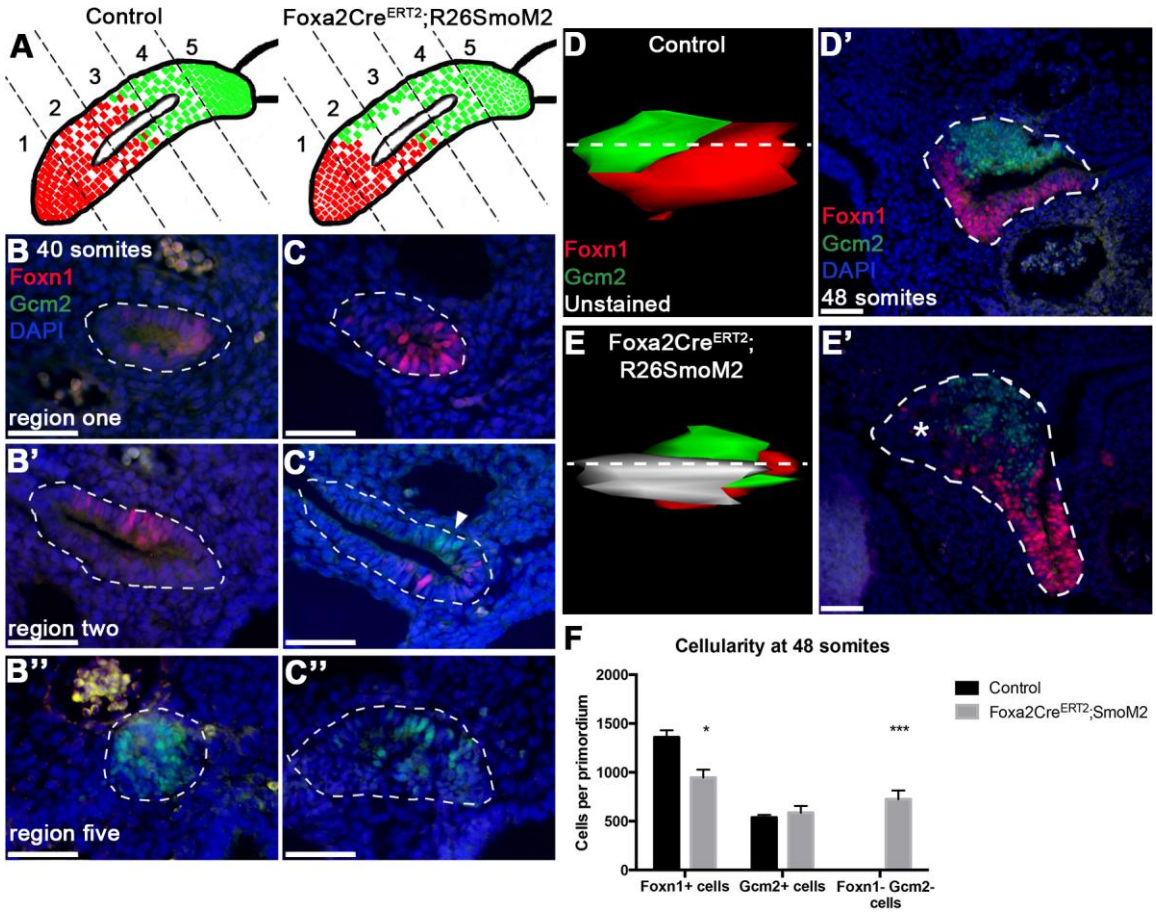

Figure 7. Ectopic activation of SHH signaling in pouch endoderm. All sections were stained with antibodies against GCM2 (green) and FOXN1 (red); primordia are outlined. **A:** Cartoons illustrating distribution of $GCM2^{+}$ and $FOXN1^{+}$ cells within the primordium for each genotype from a sagittal view. Primordia were divided into five equal regions from ventral to dorsal. White indicates cells that express neither marker. **B-C'':** Coronal sections through 40-somite stage embryos. Representative sections from regions 1 (**B,C**), 2 (**B',C'**), and 5 (**B'',C''**) are shown. Scale bar: 50 μm. **D-E':** 3-D reconstructions (**D,E**) and representative transverse sections of 48 somite primordia (**D',E'**). Dashed line indicates position of section in adjacent panel (D',E'). Asterisk indicates region of marker-negative cells. Anterior is up; dorsal surface is facing. Scale bar: 50 μm. **F:** Total number of cells in

each primordium in somite-matched mutants (n=10) and littermate controls (n=6).

mean+s.e.m. t-test *P < 0.05. ***P < 0.001.

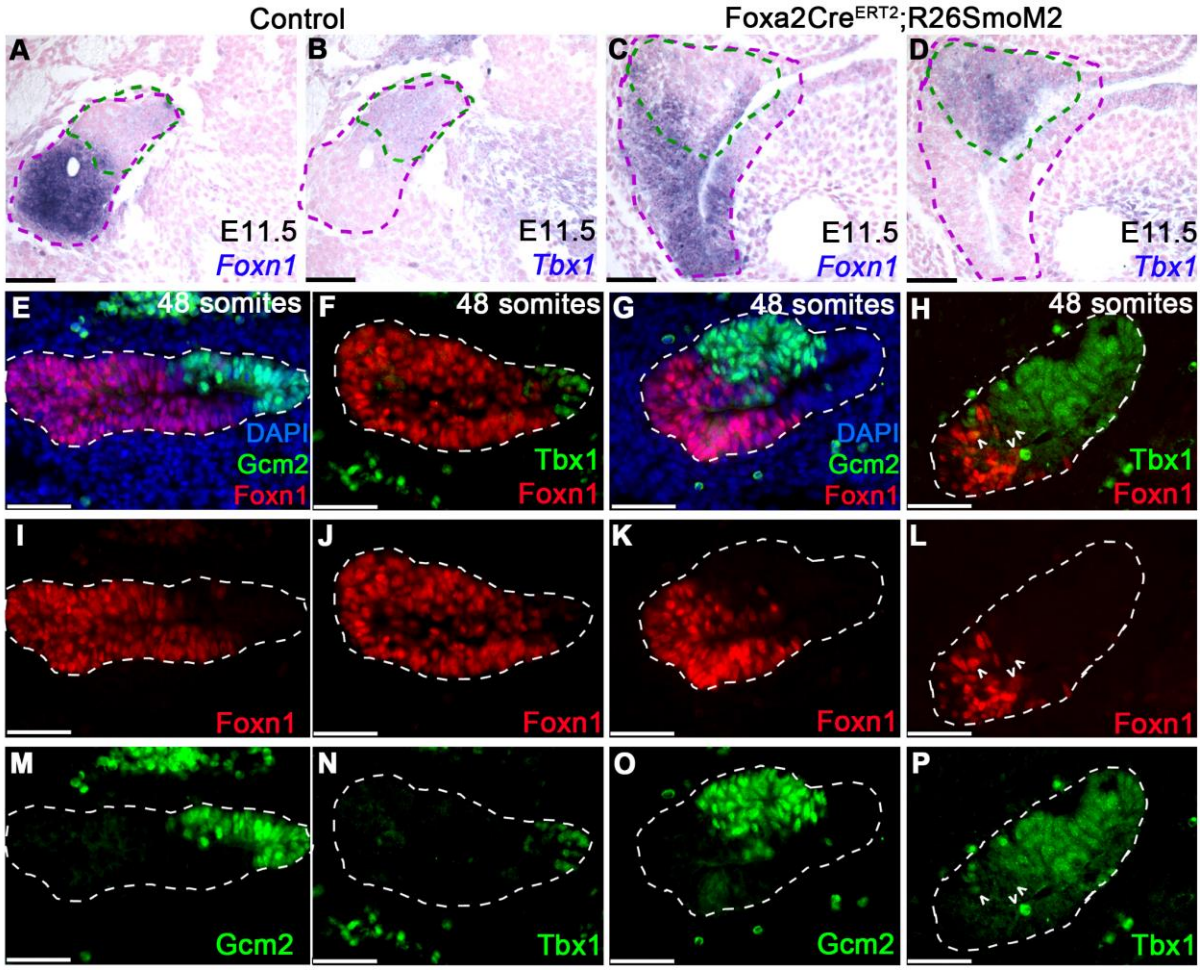

Figure 8. *Foxn1*, *Tbx1*, and *Gcm2* expression in *Foxa2Cre^{ERT2};R26SmoM2* embryos. **A-D:** Alternate transverse sections stained by ISH for *Foxn1* and *Tbx1* as marked. Primordia are outlined in magenta; *Tbx1*-positive region is traced onto both sections in green. (n = 6 per genotype) **E-P:** Serial sagittal sections stained with anti-GCM2 (green) and anti-FOXN1 (red); or anti-TBX1 (green) and anti-FOXN1 (red) as indicated. Single channels are shown below each dual-color image. Primordia are outlined. Arrowheads in **H, L** and **P** indicate cells co-labeled for TBX1 and FOXN1. (n=2/genotype). Scale bars: 50 μm.

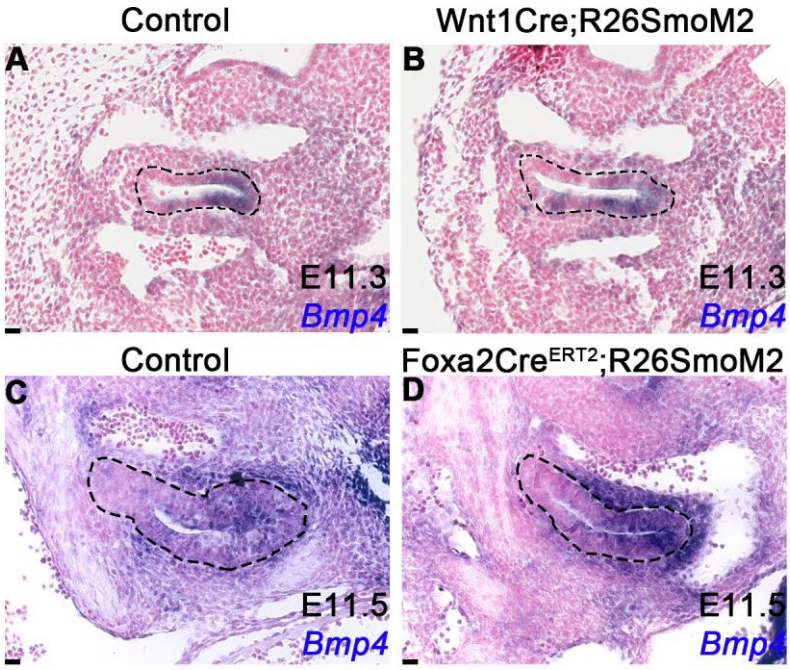

Figure 9. *Bmp4* expression is not changed after ectopic activation of SHH signaling. **A-B:** Sagittal sections through E11.3 control (**A**) and *Wnt1Cre;R26SmoM2* (**B**) primordia stained by ISH for *Bmp4*. Ventral is left. **C-D:** Sagittal sections through E11.5 control (**C**) and *Foxa2Cre^{ERT2};R26SmoM2* (**D**) primordia stained by ISH for *Bmp4*. Ventral is right. Primordia are outlined. (n=2/genotype). Scale bars: 50 μm.

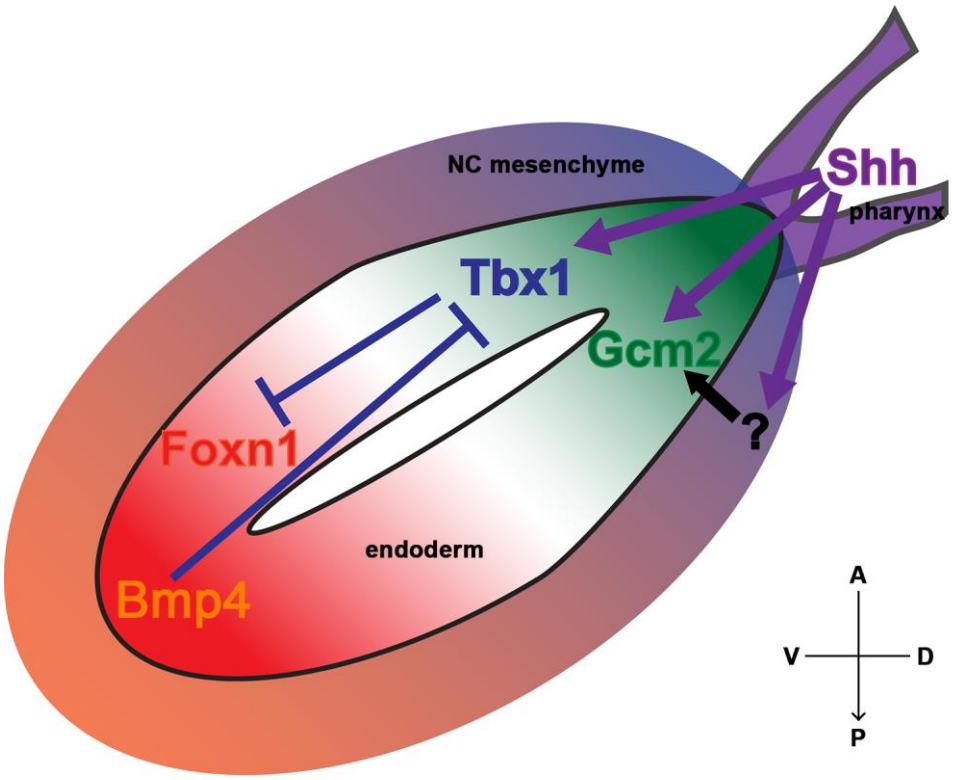

Figure 10. Model for 3rd pp patterning during initial thymus and parathyroid organogenesis. SHH signaling to the dorsal region of the 3rd pp promotes *Tbx1* expression, which, directly or indirectly, inhibits *Foxn1* expression and limits expansion of thymus fate within the pouch endoderm. SHH also independently promotes *Gcm2* expression, perhaps via *Tbx1*; additional signals from neighboring NC cells may also be required for parathyroid fate specification and *Gcm2* expression. The ventral region of the 3rd pp is protected from SHH signaling by BMP4. NC mesenchyme, endoderm, and pharynx are marked. Anterior (A), posterior (P), dorsal (D), ventral (V).

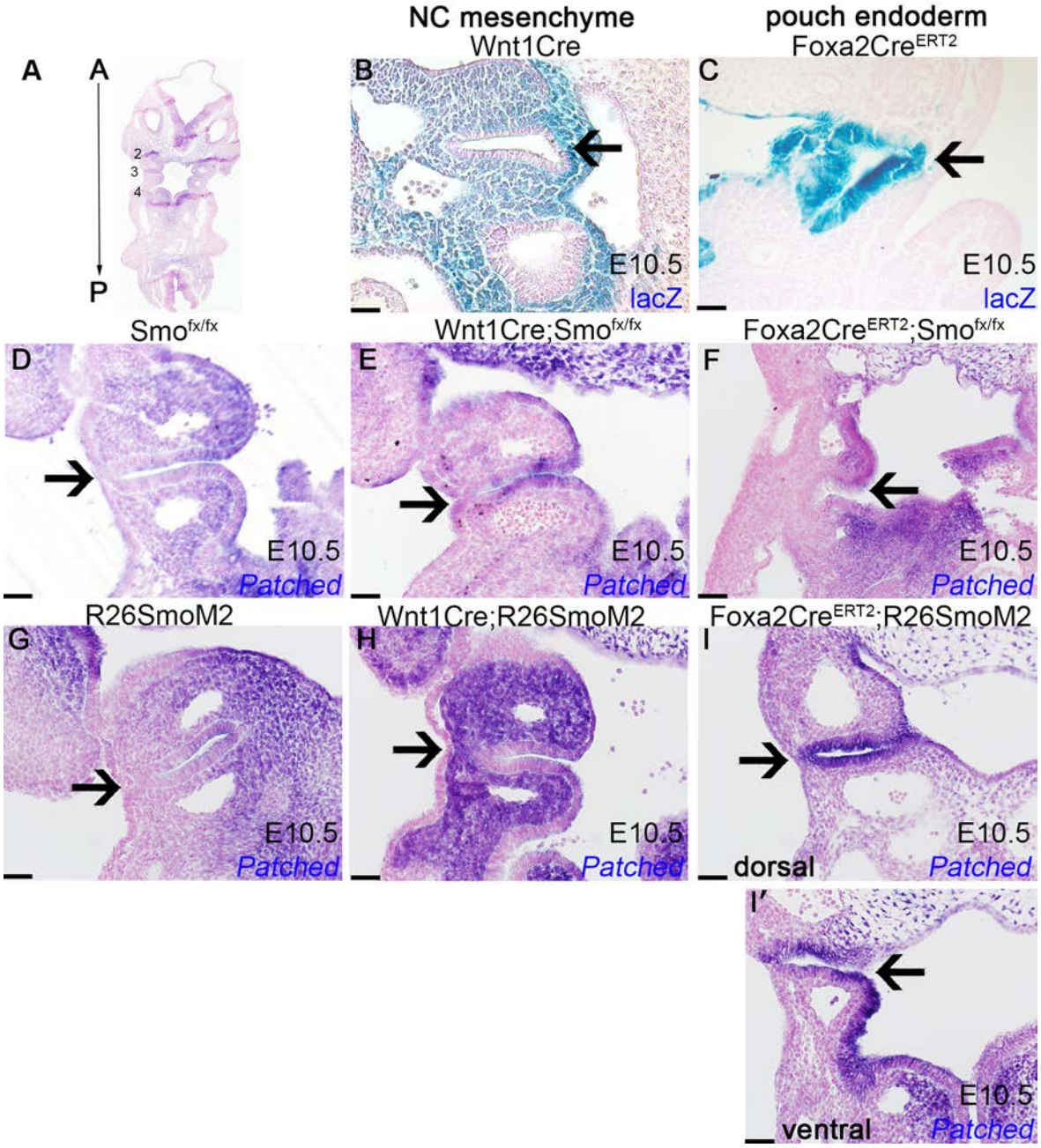

Figure S1. Validation of mouse models used in the study. Arrows in all panels indicate the 3rd pp. A: Coronal section showing anterior to posterior orientation (arrow) and locations of the 2nd 3rd and 4th pharyngeal pouches (numbers). B: Sagittal section showing activation of the R26R βgal reporter by

Wnt1Cre. C: Transverse section showing activation of the R26R βgal reporter by *Foxa2Cre*^{ERT2} after injection of tamoxifen at E5.75. D-I: Coronal sections showing SHH signaling as assayed by *Ptch1* ISH at E10.5. Cre-negative littermate controls show that SHH signaling is not uniform throughout the endoderm (D, G). SHH signaling is absent in the mesenchyme when *Smo* is deleted by *Wnt1Cre* (E). SHH signaling is absent in the endoderm when *Smo* is deleted by *Foxa2Cre*^{ERT2} (F). SHH signaling is constitutively active in the mesenchyme when *SmoM2* is activated by *Wnt1Cre* (H). SHH signaling is constitutively active in the endoderm when *SmoM2* is activated by *Foxa2Cre*^{ERT2} (I). I' shows a more ventral section from the same embryo as in I. Scale bars: 50 μm (n = 3 for panels D - I).

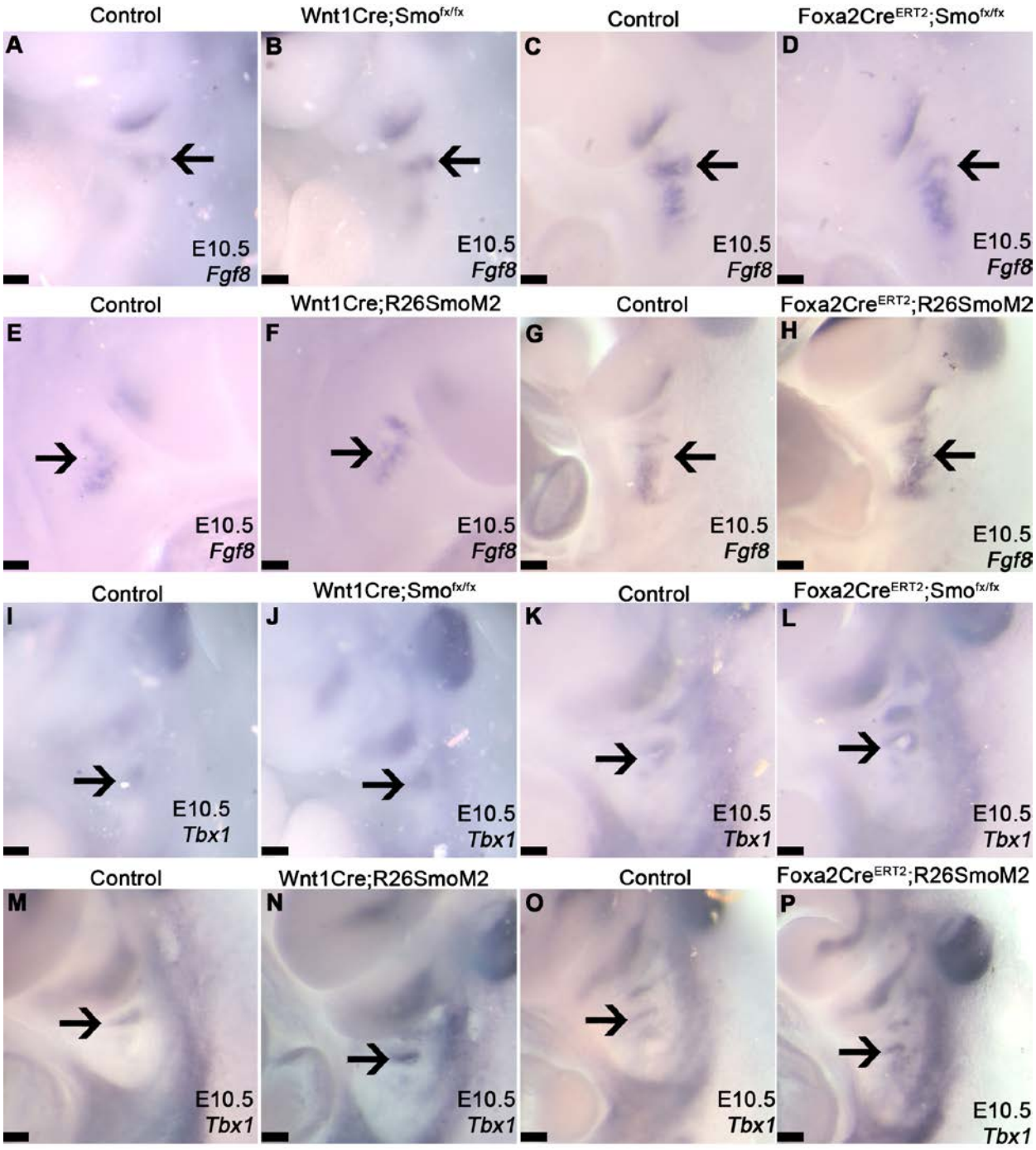

Figure S2. Markers of pharyngeal pouch patterning are unchanged at E10.5. A-H: Lateral views of whole-mount *Fgf8* ISH on mutants and littermate controls matched by somite stage at high magnification (A-D, 36 somites; E-F, 37 somites; G-H, 35 somites). Arrows indicate 3rd pharyngeal

pouch. I-P: Lateral views of whole-mount *Tbx1* ISH on mutants and littermate controls matched by somite stage at high magnification (I-L, 36 somites; M-N, 37 somites; O-P, 35 somites). Arrows indicate 3rd pharyngeal pouch. Scale bar: 100 μm, ($n \geq 4$ for all panels except H, where n = 2). Controls A, C, and K are $Cre^{neg};Smo^{fx/fx}$. Control I is $Cre^{neg};Smo^{fx/+}$. Controls E, G, M, and O are $Cre^{neg};R26SmoM2/+$.

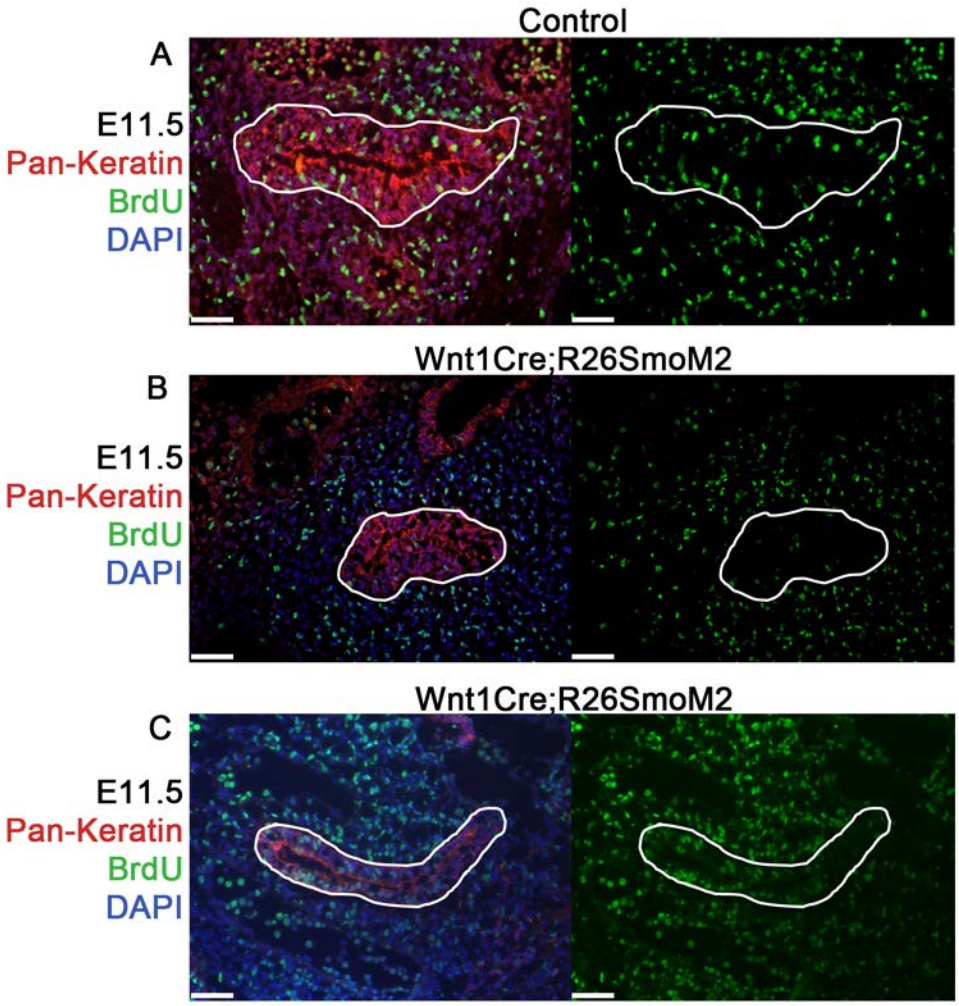

Figure S3. Proliferation in *Wnt1Cre;R26SmoM2* embryos at E11.5. A-C: Sagittal sections through E11.5 primordia stained with antibodies against BrdU (green) and Pan-Keratin (red), showing reduced proliferation in the mutants (n = 4). In all cases the primordium was clearly smaller than controls, but in some cases (B; n = 2) there were very few $BrdU^{+}$ cells in the primordium, while in others (C; n = 2) there appeared to be more, even though the epithelium clearly had not expanded. Primordia are outlined in white. Scale bar: 50 μm. (n = 4). Control A is Cre^{neg};*R26SmoM2/+*.

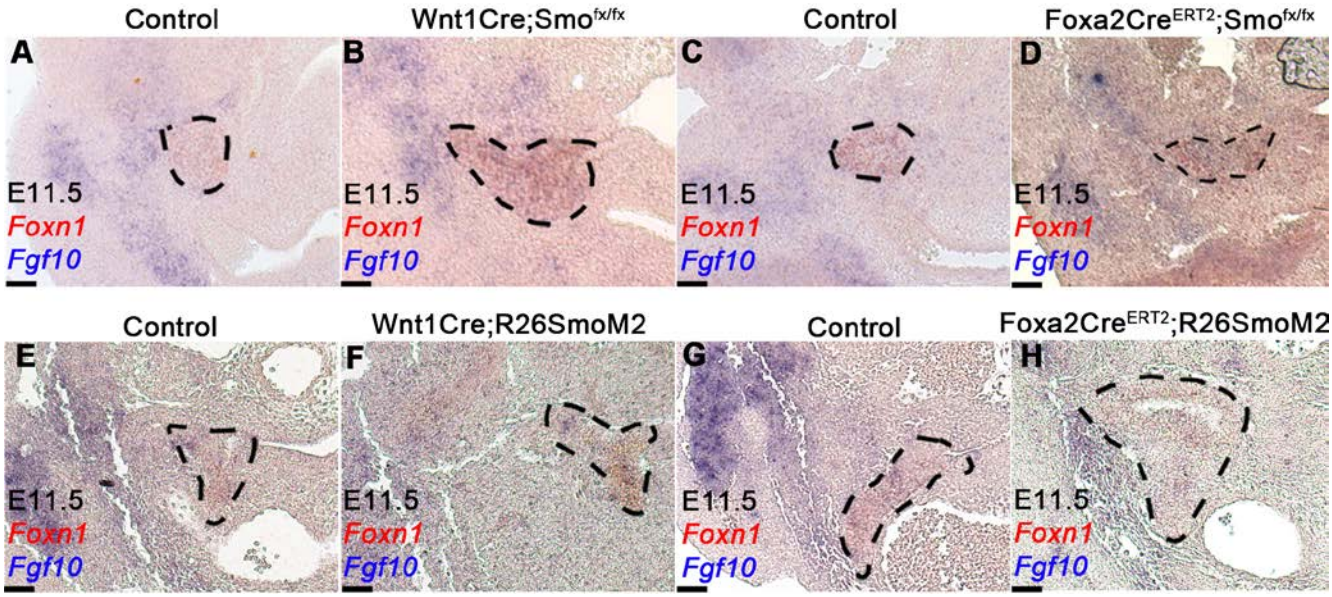

Figure S4. *Fgf10* expression in SHH signaling mutants. A-H: Transverse sections of dual-color *Foxn1* (red) and *Fgf10* (purple) ISH at E11.5. Pouch is outlined in black. Scale bars: 50 μm (n = 2 per panel, except B and H where n = 3). Controls A and C are $Cre^{neg};Smo^{fx/fx}$. Controls E and G are $Cre^{neg};R26SmoM2/+$.

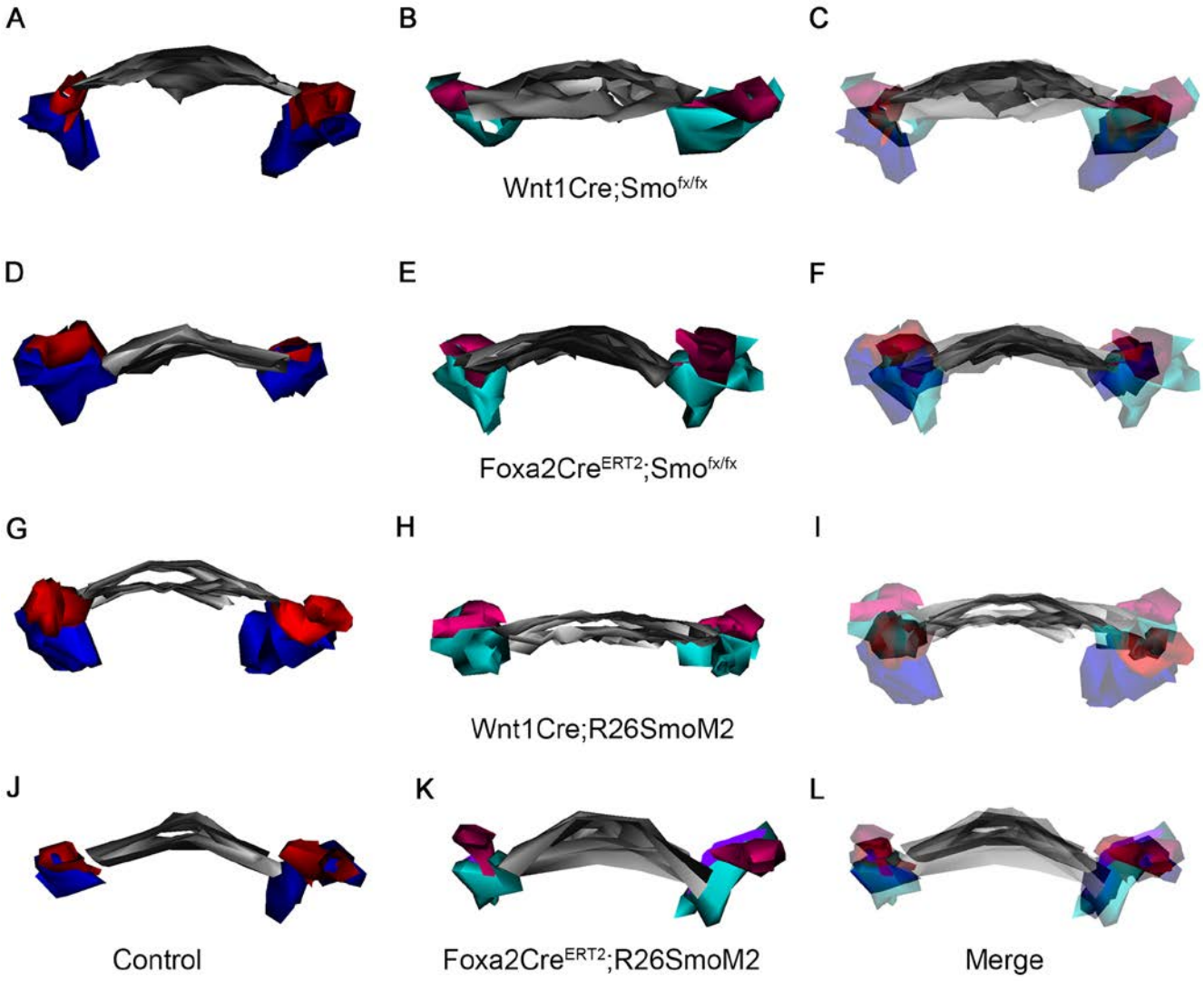

Figure S5. Pharynx shape and pouch location in SHH signaling mutants. A, D, G, J: Anterior views of 3-D reconstructions of wild type littermates at E11.5 showing the Gcm2 domain (red), the Foxn1 domain (blue), and the pharynx (gray). B, E, H, K: Anterior views of 3-D reconstructions of *Wnt1Cre;Smo*^{fx} (B), *Foxa2Cre*^{ERT2}*;Smo*^{fx} (E), *Wnt1Cre;R26SmoM2* (H), and *Foxa2Cre*^{ERT2}*;R26SmoM2* (K) embryos at E11.5 showing the Gcm2 domain (magenta), the Foxn1 domain (turquoise), and the pharynx (gray). C, F, I, L: Merged 3-D reconstructions for *Wnt1Cre;Smo*^{fx} (C), *Foxa2Cre*^{ERT2}*;Smo*^{fx}

(F), *Wnt1Cre;R26SmoM2* (I), and *Foxa2Cre^{ERT2};R26SmoM2* (L). All reconstructions were generated from transverse sections of embryos stained by dual ISH for *Foxn1* and *Gcm2* (data not shown, n = 2 per genotype). Control A is *Cre^{neg};Smo$^{fx/fx}$*. Control D is *Cre^{neg};Smo$^{fx/+}$*. Controls G and J are *Cre^{neg};R26SmoM2/+*.